AWARD NUMBER: W81XWH-14-1-0296

TITLE: Microenvironments and Signaling Pathways Regulating Early Dissemination, Dormancy, and Metastasis

PRINCIPAL INVESTIGATOR: John Condeelis

CONTRACTING ORGANIZATION: Albert Einstein College of Medicine
Bronx, NY 10461-1931

REPORT DATE: September 2015

TYPE OF REPORT: Annual

PREPARED FOR: U.S. Army Medical Research and Materiel Command
Fort Detrick, Maryland 21702-5012

REPORT DOCUMENTATION PAGE

Form Approved
OMB No. 0704-0188

1. REPORT DATE	2. REPORT TYPE	3. DATES COVERED
September 2015	Annual	1 Sep 2014 - 31 Aug 2015

4. TITLE AND SUBTITLE

Microenvironments and Signaling Pathways Regulating Early Dissemination, Dormancy, and Metastasis

5a. CONTRACT NUMBER

5b. GRANT NUMBER
W81XWH-14-1-0296

5c. PROGRAM ELEMENT NUMBER

6. AUTHOR(S)
John Condeelis, Julio Aguirre-Ghiso

E-Mail:john.condeelis@einstein.yu.edu

5d. PROJECT NUMBER
0010533520

5e. TASK NUMBER

5f. WORK UNIT NUMBER

7. PERFORMING ORGANIZATION NAME(S) AND ADDRESS(ES)

Albert Einstein College of Medicine
1300 Morris Park Ave LBBY
Bronx, NY 10461-1931

8. PERFORMING ORGANIZATION REPORT NUMBER

9. SPONSORING / MONITORING AGENCY NAME(S) AND ADDRESS(ES)

U.S. Army Medical Research and Materiel Command
Fort Detrick, Maryland 21702-5012

10. SPONSOR/MONITOR'S ACRONYM(S)

11. SPONSOR/MONITOR'S REPORT NUMBER(S)

12. DISTRIBUTION / AVAILABILITY STATEMENT

Approved for Public Release; Distribution Unlimited

13. SUPPLEMENTARY NOTES

N/A

14. ABSTRACT

We devoted majority of the effort to SA1 and optimizing methods that impact both aims. SA1 is to understand the intrinsic mechanisms of dissemination by early-progressed cancer cells and how the microenvironment in these primary sites named P-TMEM (**P**rimary **T**umor **M**icro**e**nvironment of **M**etastases) contribute to early dissemination. We now have new data suggesting that a signature of early dissemination markers consisting on $HER2^{HI}$/p-$ATF2^{LO}$/E-$cadh^{LO}$ could identify motile early-progressed tumor cells and predict for dissemination. We further show that mammary tissue macrophages and $HER2^{HI}$/p-$ATF2^{LO}$/E-$cadh^{LO}$ tumor cells cooperate to disseminate early. This further supports our hypothesis that even in early cancer lesions macrophages and tumor cells assemble with endothelial cells a TMEM structure. We have also made progress in generating a standardized triple staining that captures all these cell types in all tissues and we have been able to document using intravital imaging the process of intravasation in early cancer lesions. Our work revealed that the presence of intraepithelial macrophages in DCIS samples could accurately predict dissemination in 70% of the cases of patients with bone marrow DTCs (**D**isseminated **T**umor **C**ells). SA2 focuses on elucidate how S-TMEM (**S**econdary **T**umor **M**icro**e**nvironment of **M**etastases) contributes to the dormancy phase of early DTCs. Our new data show that depletion of macrophages during early dissemination steps significantly reduces metastasis that develop into the late stages of progression, providing functional support for macrophages in P- and S-TMEM structures in metastasis development. We also found that early DTCs appear to undergo a p38 independent dormancy and remain mesenchymal in secondary organs. In contrast, in animals with overt tumors p38 inhibition resulted in an awakening of dormant DTCs in lungs, that now have a mixture of early and late disseminated tumor cells. Progress has also been made in devising a sorting protocol to isolate CFP+/HER2+ DTCs from lungs and CTCs in the MMTV-Neu-CFP model and we have also devised new strategies to identify the early and late gene signatures in DTCs proposed in our grant. Overall we have made significant progress and we do not foresee having to alter our specific aims in any way.

15. SUBJECT TERMS
dormancy, early dissemination, EMT, macrophages, TMEM

16. SECURITY CLASSIFICATION OF:			**17. LIMITATION OF ABSTRACT**	**18. NUMBER OF PAGES**	**19a. NAME OF RESPONSIBLE PERSON**
					USAMRMC
a. REPORT	**b. ABSTRACT**	**c. THIS PAGE**			**19b. TELEPHONE NUMBER** *(include area code)*
"U"	"U"	"U"	"UU"	50	

Table of Contents

The text of the report must include all sections addressed in the table of contents to include the following. **DO**include the bolded section headings, but **DO NOT** include the *italicized* descriptions of section contents in your submitted reports.

1. **INTRODUCTION:**

We have evidence for the existence of a structure called tumor microenvironment of metastasis or TMEM, which is composed by a proangiogenic macrophage a, a Mena overexpressing tumor cell and an endothelial cell where the three cell complex is in direct contact with a blood vessel wall. We detected primary tumor TMEM (**P-TMEM)** in pre-malignant lesions. The P-TMEM is required to support early dissemination of pre- malignant neoplastic cells (early DTCs). We further hypothesize that after extravasation at secondary site TMEM (**S-TMEM**), in order to exit dormancy a stable S-TMEM structure needs to be maintained and that early DTCs cannot sustain its assembly possibly because they lack a persistent proangiogenic MΦ recruiting program. Our *rationale* is that by understanding early dissemination and dormancy of DTCs we will find ways to eradicate dormant DTCs and prevent metastasis.

2. **KEYWORDS:** TMEM, DTC, dormancy, dissemination intravasation, extravasation

3. **ACCOMPLISHMENTS:**

- **What were the major goals of the project?**

Our original specific aims are:

1. Test how ErbB2high/P-p38low MECs assemble P-TMEM during early dissemination.

2. Test the role of S-TMEM in regulating early DTC dormancy.

- **What was accomplished under these goals?**

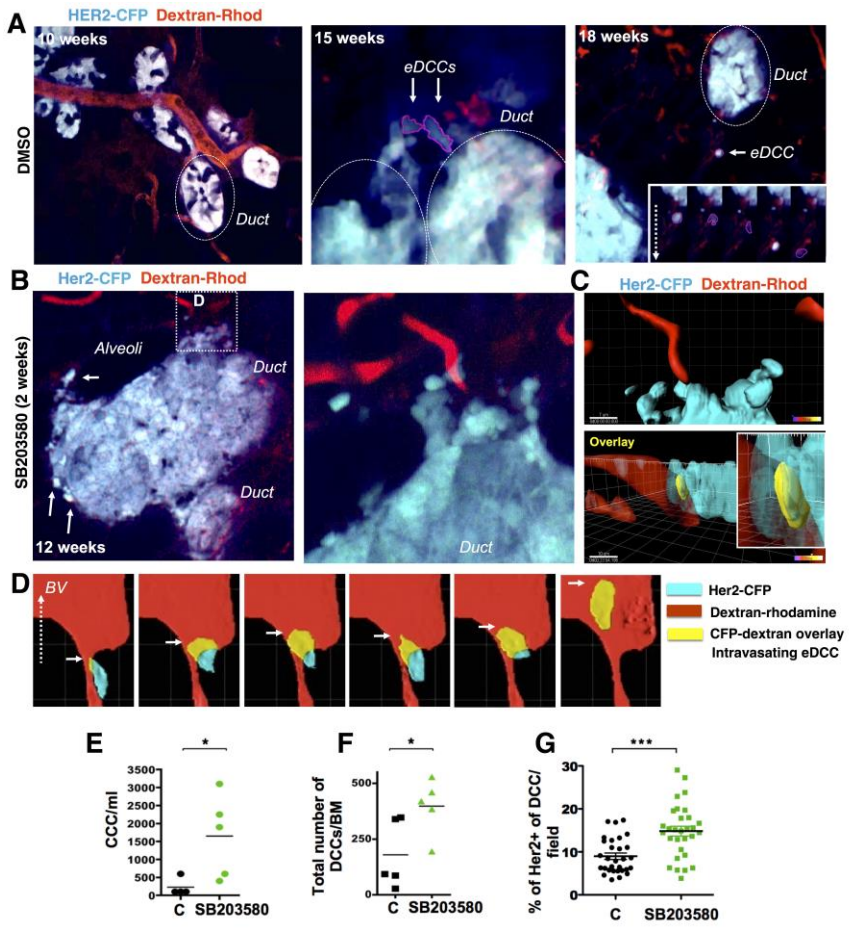

Fig 1. High resolution 2-photon intra-vital imaging of early dissemination. (A) Stills from intra-vital movies of 10 (left), 15 (middle) and 18 (right) weeks old mammary glands of MMTV-HER2-CFP mice. Blue-white signal pinpoints the CFP+ cells while rhodamine-dextran injected i.v. is the vasculature. Inset in the left panel shows a detail of a CFP+ duct (dotted line). The arrows and outlines in the middle 15 wks panel shows CFP+ cells actively microinvading and translocating. Sequence inset in the right 18 wks panel shows active microinvasion and travel of a early cancer cells. Dotted arrow= down director of movement. **(B)** Stills from intra-vital movies of a duct from an MMTV-HER2-CFP mice treated with SB203580 for 2 weeks. **(C)** The same projection as in C lright panel but rotated to show the interaction (yellow) between early cancer cells (CFP) and blood vessels (red). **(D)** frames (every 10 min) of a 3D computer generated reconstruction of a movie showing an intravasation event. **E**, circulating cancer cell (CCC) measurements in blood in control or p38 inhibitor SB203580-treated animals. F and G, same as in E but the cells scored were bone marrow DCCs (F) and DCCs in lungs (G).

Specific Aim 1. Sites one (Mount Sinai) and two (Einstein) worked closely on the accomplishments of the following key findings. This work was accomplished either by direct experimentation by personnel of both groups at one or the other site or through the sharing of critical information on methodologies or techniques that allowed accomplishing the goals in Aim 1 primarily. Much of the effort in Einstein was devoted to developing technology and to image premalignant mammary glands and the process of intravasation. This work, which is represented in bullets 1-4 is now part of a manuscript invited to revise and resubmit to *Nature* (see attached manuscript in its first version submitted to Nature and title in bullet #8). We also provide additional data of the imaging analysis and computational processing of the intravital imaging below.

1. Design of a flat window device that allows the imaging of pre-malignant lesions in the tissue fat pad of MMTV-Neu-CFP mouse model.

2. Inhibition of p38α/β *in vivo* showed increased motility of pre-malignant MMTV-Neu-CFP cells.

3. Identification of a signature consisting on $HER2^{HI}$/p-$ATF2^{LO}$/E-$cadh^{LO}$ that marks motile early-progressed tumor cells and predicts for dissemination.

4. Validation of the P-TMEM structure in the MMTV-Neu-CFP mouse model.
5. Detection and identification of macrophage subtyupe linked to early dissemination (Tie2+/VCAM-/CD206+ mammary tissue macrophages)
6. Detection of intraepithelial macrophages predicts dissemination in DCIS samples.
7. Macrophages in early lesions induce an EMT and promote early dissemination.
8. Kathryn L. Harper, Maria Soledad Sosa, Hedayatollah Hosseini, David Entenberg, Alvaro Avivar-Valderas, Chandandaneep Nagi, Roger J. Davis, Eduardo F. Farias, John Condeelis, Christoph Klein, and Julio A. Aguirre-Ghiso. Mechanism of early dissemination and metastasis during early stages of HER2+ mammary cancer. Invited to resubmit to Nature (2016).

High-resolution live-cell imaging reveals the motility and intravasation of early disseminating cancer cells. Our goal was to test how ErbB2high/P-p38low MECs assemble P-TMEM during early dissemination. However, this required first determining the kinetics and model of motility of early cancer cells. Our data in the paper attached by Harper et al., revealed that HER2^{+}/E-cad^{lo}/P-p38^{lo}/CK8/18+ early cancer cells are motile and invasive, but these data were inferred from static images (**Figs1and 2 of the manuscript**). Thus, we next used high-resolution intra-vital imaging[26] of MMTV-HER2-CFP transgenic mice to unambiguously record at single-cell level resolution the micro-invasive capacity of early HER2^{+} invasive cancer cells (**Fig1 in this report**). To monitor cancer cell motility in early lesions we designed a mammary imaging window to accommodate the depth and lax consistency of the mammary fat pad tissue. 2-photon imaging of regions of the ductal tree in vehicle treated HER2-CFP mice where the vasculature is revealed by i.v. delivered dextran-rhodamine [26]) showed that early cancer cell motility and local invasion was infrequent at 10 weeks when the ducts in the MMTV-HER2-NDL5-CFP model still display normal ductal architecture (**Fig1A, left)**. However, at 15 and 18 weeks of progression when early lesions are observed, local invasive CFP+ cell translocation and cell motility were detectable even in an imaging area that captures a very small fraction of the transgenic mammary tree (**Fig1A middle and right**). At this time we could also detect CFP+ cell translocation and exit from lesions into the stroma (**Fig1A, right**). Histological sections of these lesions and double staining for HER2 and GFP (CFP and GFP share the same immune epitope) revealed that the CFP positive cells in the intraepithelial lesions or already micro-invading were in their majority (>90%) HER2 positive regardless of their location (**not shown**). Thus, CFP reports faithfully for HER2 overexpressing cells. Forcing a HER2^{+}/E-cad^{lo}/P-p38^{lo} profile using a p38α/β inhibitor revealed an enhancement of the motile and invasive phenotype observed in basal conditions (**Fig1A**) as now cells showed the formation of cell protrusions, intra-ductal migration, locomotion along ductal walls and local invasion and intravasation (**Fig1B, C and D**).

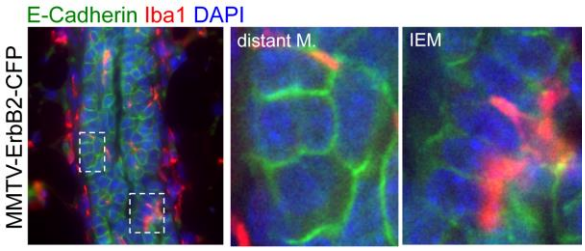

Figure 2. Paraffin embedded sections of 7 week old MMTV-ErbB2-CFP mammary glands were stained for E-Cadherin and the macrophage marker Iba1. Detail on the right shows that E-Cadherin is disrupted and reduced in early cancer cells adjacent to intra-epithelial macrophages.

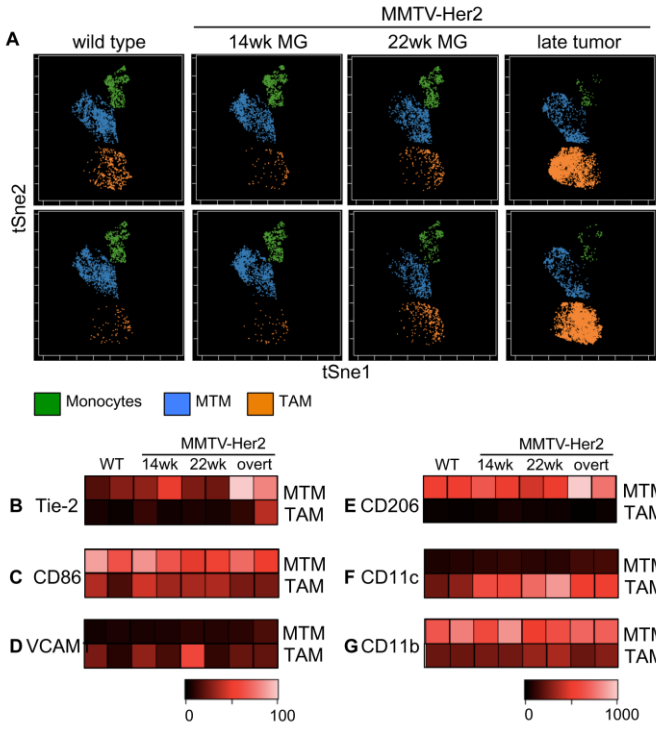

Figure 3. Phenotypic profiling of macrophages in early mammary cancer lesions. Whole mammary glands from FVB wild type mice or 14 and 20 week old pre-malignant MMTV-ErbB2 mice and invasive tumors from MMTV-ErbB2 mice were analyzed by mass cytometry against 36 markers. To analyze macrophages and monocytes, we gated out doublets, dead cells, non-hematopoietic cells (CD45), non T- and B-Cells (CD4, CD19) and non-neutrophils (Gr1) and then analyzed CD64+ CD1b+ cells. A: Visne plots of Ly6C+ monocytes, CD206+ mammary tissue macrophages (MTMs) and VCAM+ tumor associated macrophages (TAMs). Two individual animals per group were analyzed (top and bottom row). B-G: Heat plot analysis for different markers in the identified subpopulations are shown.

Unlike in 3D cultures (not shown), we did not observe collective cell migration *in vivo* and cells displayed more ameboid-like features [27]. High-resolution imaging and 3D reconstruction of the micro-invasion and intravasation events showed unambiguously how individual cells micro-invaded outwards from the ductal pre-malignant lesions and invaded through the stroma (**Fig1C**) entering the lumen of blood vessels that is revealed by the overlay of the CFP signal an the dextran-rhodamine signal that only occupies the luminal space (**Fig1C**). These high-resolution intra-vital imaging studies document early cancer cell motility and micro-invasion and intravasation.

To confirm that the intravasation documented in the movies was successful we measured CK8/18+ and/or HER2+ pre-malignant cancer cells in peripheral blood, in BM and lungs of MMTV-HER2 mice carrying early lesions (**Fig1E-G**). We found that a 2-week treatment with SB203580 significantly increased the numbers of CK8/18+ circulating cancer cells. This was followed by an increase in the total number of CK8/18+/HER2^{+} eDCCs in the BM and HER2^{+} eDCC in lungs (**Fig1F-G**). The detection of CK8/18 alone or with HER2 in BM eDCCs argues that these are epithelial cells and not leukocytes with ectopic expression of HER2 due to MMTV aberrant activation as reported previously[3]. The median number of eDCCs in the BM compartment is equivalent to ~1.3 eDCCs/ 10^6 BM host cells in control groups and ~8 eDCCs/10^6 BM host cells in SB203580 treated animals. We did find that some eDCCs were CK8/18+ and HER2-negative as found by Hosseini et al. (not shown). However, when considering the HER2^{+}/CK8/18+ early DCCs the stimulation of dissemination by SB203580 was significant (**Fig1F-G**). The imaging of EL showing intravasation followed by the detection of CCCs and DCCs confirm that CK8/18+ early HER2^{+} cancer cells intravasate, disseminate and can be further stimulated to exit the early lesions by forcing an EMT-like^{high}/p38^{lo} profile.

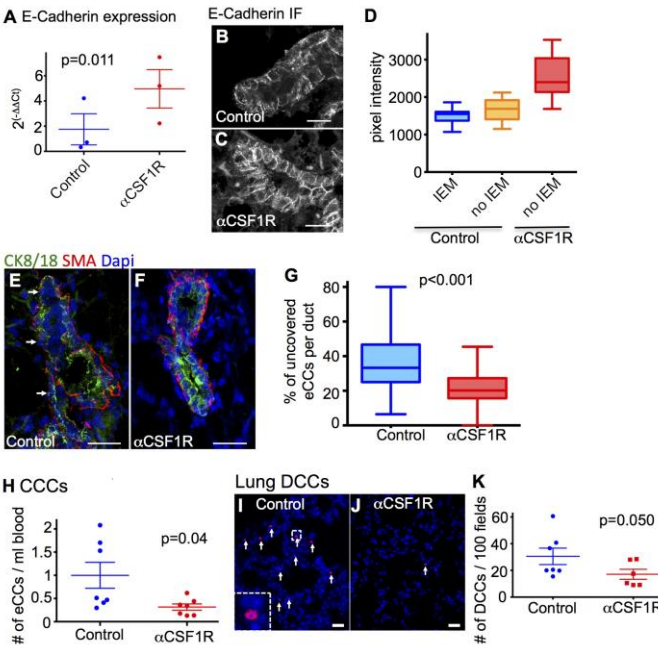

Figure 4. Macrophage depletion during pre-malignant stages prevents early cancer cell dissemination. 20 week old pre-malignant MMTV-ErbB2 mice were treated with the anti CSF-1Ra ASF98 antibody and animals were harvested after two weeks with no signs of invasive carcinoma. E-Cadherin expression in whole mammary glands was determined by immunofluoresence staining against E-Cadherin of mammary gland sections (A) and RealTime PCR of whole mammary gland lysates (B). E-Cadherin signal intensity was measured in regions of cell junctions, dependent on the presence of intra-epithelial macrophages (IEM) (D). Pre-malignant mammary glands were stained against (E,F) and the percentage of early cancer cells not covered by myoepithelium was quantified (G). Circulating early cancer cells were quantified by harvesting peripheral blood and determining the amount of ErbB2 and CK8/18 positive eCCs per mL blood (H). Disseminated early cancer cells were quantified by staining lung sections against ErbB2 (I,K) and quantifying the average of ErbB2+ cells per 100 fields (K). CCCs, circulating cancer cells. DCCs disseminated cancer cells

2. Investigate the role of S-TMEM in regulating early DTC dormancy.

This section was performed in the Aguirre-Ghiso lab (partnering lab) with support of our expertise and reagents. We thus reproduce relevant sections from the progress report from our partnering team. The intravasation shown in Fig1, may also be the consequence of macrophages assembling P-TMEM and further enhancing the EMT. To asses this possibility, we stained macrophages in sections in MMTV-ErbB2-CFP mice and could reproduce our finding that macrophages enter pre-malignant mammary ducts (not shown). We also found that early cancer cells neighboring intra-epithelial macrophages show low levels of E-Cadherin (**Fig.2**), indicating that intra-epithelial macrophages might induce an EMT in pre-malignant MECs. We then analyzed the phenotype of macrophages in FVB wild type or pre-malignant MMTV-ErbB2 mammary glands as well as in MMTV-ErbB2 invasive tumors by mass flow cytometry (CyTOF – **Fig3**) and found that wild type and pre-malignant mice predominantly contained mammary tissue but not tumor-associated macrophages and that these mammary tissue macrophages matched the Tie2^{high}, CD11c^{low}, CD206^{+} signature of TMEM macrophages recently described for invasive tumors[3] (**Fig.3**) indicating that a P-TMEM which drives early dissemination might be functional in pre-malignant stages as well.

We next tested whether macrophages functionally contribute to early dissemination by depleting macrophages from pre-malignant MMTV-ErbB2 mice using an antibody against CSF1Rα for two weeks and sacrificed animals before these developed signs of invasive tumors. We found that macrophage depletion during pre-malignant stages restored overall E-Cadherin expression and E-Cadherin signal intensity (**Fig.4A-D**) and

normalized the myoepithelium covering pre-malignant ducts **Fig.4E-G**). Importantly, the number of circulating MECs and disseminated MECs in the lung was significantly reduced when macrophages had been depleted (**Fig.4H-K**).

Conclusions: First we confirmed that inhibition of p38α/β signaling by treatment of the new MMTV-Neu-CFP mice with SB203580 recapitulated the previously effect shown in the MMTV-Neu mice (no tag). These results also revealed in real time and live imaging the dissemination process as never before documented. These data support the hypothesis that p38 inhibition favors a motile phenotype that propels early dissemination. These findings are part of 2 manuscripts now in the process of review (Appendix I and II). The additional evidence showed that intraepithelial macrophages also occur in the MMTV-Neu-CFP mice and we characterize these macrophages as mammary tissue macroiphages[4] and showed that these are vital for disrupting the ductal epithelial structures, favoring an EMT and favoring early dissemination

- **What opportunities for training and professional development has the project provided?**

Nothing to report.

- **How were the results disseminated to communities of interest?**

Nothing to report.

- **What do you plan to do during the next reporting period to accomplish the goals?**

We will quantify the number of events that show intravasation dynamics of pre-malignant DTCs into blood vessels in DMSO- and SB-treated animals. Specifically, we will quantify speed, frequency and mode (single cells vs. cohorts and/or streaming) of local invasion and intravasation. So far our analysis has been performed with a imaging resolution that enables us to detect single cells by doing z-stack of 5 um. We will increase the number of images taken per region to detect 1 um of thickness. With this type of resolution we will perform 3D reconstructions to detect with high quality the body and protrusions of any given cell. This undoubtedly will help us to identify the whole cell along its trajectory. Once we have established the optimal settings for visualization in vivo we will proceed by using the MMTV-PyMT- EGFP-c- fms-CFP mouse model. The latter, will allow us to detect the interactions of macrophages (CFP) with tumor cells (GFP). We are also optimizing the triple staining detection of TMEM structures by IHC and this will allow direct comparison of fixed tissue sections with the intravital multiphoton imaging that will lead to a standard measure of P-TMEM and S-TMEM quantification in FFPE tissue.

4. **IMPACT:**

- **What was the impact on the development of the principal discipline(s) of the project?**

TMEM test: TMEM is composed of the stable direct interaction of a pro-angiogenic Tie2-high, VEGF-high, MRC1-high macrophage, endothelial cell and MenaCalc positive tumor cell. Further study led to the discovery that TMEM is the only doorway for tumor cell entry into blood vessels (1). In a major discovery, TMEM were found in all primary and secondary sites and in all stages of breast cancer progression making TMEM the common dissemination marker in all breast tumors and their associated distant sites. TMEM score (determined in FFPE tissue) has been shown to be superior in predicting distant recurrence to that of OncotypeDX and IHC4 and demonstrates higher accuracy and sensitivity. TMEM score has also been shown to be independent of, and to contain significant prognostic information beyond that captured by, OncotypeDX and IHC4 (2,3).

1. Harney AS, Arwert EN, Entenberg D, Wang Y, Guo P, Qian BZ, Oktay MH, Pollard JW, Jones JG, Condeelis JS. (2015). Real-Time Imaging Reveals Local, Transient Vascular Permeability, and Tumor Cell Intravasation Stimulated by TIE2hi Macrophage-Derived VEGFA. **Cancer Discovery**. 5(9):932-43. PMID: 26269515 / PMCID: PMC4560669.

2. Robinson BD, Sica GL, Liu YF, Rohan TE, Gertler FB, Condeelis JS, Jones JG. (2009). Tumor microenvironment of metastasis in human breast carcinoma: a potential prognostic marker linked to hematogenous dissemination. **Clinical Cancer Research**. 15(7):2433-41. PMID: 19318480 / PMCID: PMC3156570.

3. Rohan TE, Xue X, Lin HM, D'Alfonso TM, Ginter PS, Oktay MH, Robinson BD, Ginsberg M, Gertler FB, Glass AG, Sparano JA, Condeelis JS, Jones JG. (2014). Tumor microenvironment of metastasis and risk of distant metastasis of breast cancer. **Journal of the National Cancer Institute**. 106(8). PMID: 24895374 / PMCID: PMC4133559.

- **What was the impact on other disciplines?**

Unknown.

- **What was the impact on technology transfer?**

Nothing to report

- **What was the impact on society beyond science and technology?**

Nothing to report

5. **CHANGES/PROBLEMS:**

- **Changes in approach and reasons for change**

Nothing to report

- **Actual or anticipated problems or delays and actions or plans to resolve them**

Nothing to report

- **Changes that had a significant impact on expenditures**

Nothing to report

- **Significant changes in use or care of human subjects, vertebrate animals, biohazards, and/or select agents**

Nothing to report

- **Significant changes in use or care of human subjects -** Nothing to report
- **Significant changes in use or care of vertebrate animals. -** Nothing to report
- **Significant changes in use of biohazards and/or select agents -** Nothing to report

6. **PRODUCTS:**

-Nothing to report

- **Publications, conference papers, and presentations**
- **Journal publications.**

1. Kathryn L. Harper, Maria Soledad Sosa, Hedayatollah Hosseini, David Entenberg, Alvaro Avivar- Valderas, Chandandaneep Nagi, Roger J. Davis, Eduardo F. Farias, John Condeelis, Christoph Klein, and Julio A. Aguirre-Ghiso. Mechanism of early dissemination and metastasis during early stages of HER2+ mammary cancer. Invited to resubmit to Nature (2016).

- **Books or other non-periodical, one-time publications.**

Nothing to report

- **Other publications, conference papers, and presentations.**

Nothing to report

- **Website(s) or other Internet site(s)**

Nothing to report

- **Technologies or techniques**

  Nothing to report

- **Inventions, patent applications, and/or licenses**

  Nothing to report

- **Other Products**

  Nothing to report

7. **PARTICIPANTS & OTHER COLLABORATING ORGANIZATIONS**

- **What individuals have worked on the project?**
- *Provide the following information for: (1) PDs/PIs; and (2) each person who has worked at least one person month per year on the project during the reporting period, regardless of the source of compensation (a person month equals approximately 160 hours of effort). If information is unchanged from a previous submission, provide the name only and indicate "no change."*

Name:	John Condeeis
Project Role:	PI
Researcher Identifier (e.g. ORCID ID):	N/A
Nearest person month worked:	0.36
Contribution to Project:	Dr. Condeelis will supervise all work at Einstein. This will focus on the imaging and quantification of early disseminating cells and macrophage interactions using the *MMTV-ErbB2-CFP* and *MMTV-PyMT-EGFP-c-fms-CFP* mice. The Einstein Team, will carry the *MMTV-PyMT-EGFP-c-fms-CFP* colony, imaging early dissemination of ErbB2-CFP MECs and P-TMEM formation in untreated mice or mice where ErbB2 and p38 will be inhibited or macrophages depleted.
Funding Support:	NIH: Signal Transduction & Actin During Amoeboid Chemotaxis NIH: Tumor Microenvironments Determining Migration, Dissemination and Dormancy NIH: In Vivo Multiphoton Imaging of Complex Cancer Cell Behaviors NIH: Motility and Invasion NIH: Novel approach to study intravasation in primary human breast cancer Cells NIH: Mechanisms of lymphatic metastasis in melanoma
Name:	Yarong Wang
Project Role:	Associate
Researcher Identifier (e.g. ORCID ID):	N/A
Nearest person month worked:	0.84

Contribution to Project:	Ms. Wang is the senior technician in the mouse house of the multiphoton microscope laboratory that Dr. Condeelis directs at Einstein. She will supervise all mouse colony maintenance and preparation for intravital imaging.
Funding Support:	Gruss-Lipper Integrated Imaging Program Biophotonics Endowment

- **Has there been a change in the active other support of the PD/PI(s) or senior/key personnel since the last reporting period?** *Nothing to report.*
- **What other organizations were involved as partners?**

Provide the following information for each partnership:

- **Organization Name:** Ichan School of Medicine at Mount Sinai
- **Location of Organization:** One Gustave L. Levy Place *New York, N Y 10029*
- **Partner's contribution to the projec**t *:* As listed on the progress report submitted by Dr. Julio Aguirre-Ghiso
- **Financial support;** Nothing to report.
- **In-kind support** : Nothing to report.
- **Facilities** Nothing to report.
- **Collaboration:** As listed on the progress report submitted by Dr. Julio Aguirre-Ghiso
- **Personnel exchanges** *Nothing to report.*
- **Other.** *Nothing to report.*

8. **SPECIAL REPORTING REQUIREMENTS**

- **COLLABORATIVE AWARDS:** *For collaborative awards, independent reports are required from BOTH the Initiating PI and the Collaborating/Partnering PI. A duplicative report is acceptable; however, tasks shall be clearly marked with the responsible PI and research site. A report shall be submitted to https://ers.amedd.army.mil for each unique award.*

Mechanism of early dissemination and metastasis during early stages of HER2+ mammary cancer.

Kathryn L. Harper[1#], Maria Soledad Sosa[1#]*, Hedayatollah Hosseini[2], David Entenberg[4], Alvaro Avivar- Valderas[1], Chandandaneep Nagi[1], Roger J. Davis[3], Eduardo F. Farias[1], John Condeelis[4], Christoph Klein[2], and Julio A. Aguirre-Ghiso[1]*

[1]Division of Hematology and Oncology, Department of Medicine, Department of Otolaryngology, Department of Oncological Sciences, Tisch Cancer Institute, Black Family Stem Cell Institute, Mount Sinai School of Medicine, New York, NY 10029, USA. [2]Experimental Medicine and Therapy Research Faculty of Medicine University of Regensburg, 93053 Regensburg, Germany. [3]Howard Hughes Medical Institute, University of Massachusetts Medical School, MA 01605, USA. [4]Department of Anatomy and Structural Biology, Integrated Imaging Program, Gruss Lipper Biophotonics Center, Albert Einstein College of Medicine, 1300 Morris Park Ave, Bronx, NY 10461, USA.

[*]*Correspondence to:* Maria Soledad Sosa and Julio A. Aguirre-Ghiso, Division of Hematology and Oncology, Department of Medicine, Head and Neck Cancer Research Program, Department of Otolaryngology, Mount Sinai School of Medicine, New York, NY, 10029. Phone: 212-241-9582 Fax: 212-241-4096 Box: 1079 E-mails: maria.sosa@mssm.edu, julio.aguirre-ghiso@mssm.edu

# Denotes equal contribution.

Running title: Signaling pathways regulating early dissemination

SUMMARY

The mechanisms that produce early-disseminated cancer cells (eDCC) during early stages of breast cancer are poorly understood. Here we show that during early mammary cancer, when only ADH or DCIS lesions are present, there is a sub-population of HER2+ early cancer cells that are invasive and disseminate to target organs. These eDCC were $HER2^{+}$/P-$ATF2^{lo}$/E-$cadherin^{lo}$, and were found also in human DCIS samples. Further, eDCCs underwent a Wnt-dependent EMT-like response that was reversed by HER2 or Wnt signaling blockade. Intra-vital imaging of transgenic HER2-CFP early lesions revealed that eDCC precursors locally invade, intravasate and circulate to target organs. Surprisingly, although the majority of eDCCs are non-proliferative, they can still initiate metastasis. We conclude that during stages of cancer considered broadly non-invasive, some HER2+ cancer cells can aberrantly activate an invasive morphogenetic program causing early dissemination. These eDCCs carry latent metastatic initiating capacity, which impacts our understanding of metastasis onset and how it might be targeted effectively.

INTRODUCTION

Metastasis is the leading cause of breast cancer (BrCa) related deaths and can often occur after prolonged periods of latency (>20 years), possibly due to the existence of quiescent/dormant disseminated cancer cells (DCC) [1,2]. Active and dormant DCCs may contribute to the phenotypic and genetic heterogeneity of metastasis initiating cells, timing of metastasis and therapy failure [2,3]. However, the source of DCCs contributing to this heterogeneity is not fully known and central to preventing metastasis related deaths.

More importantly, during what point in cancer evolution do DCCs originate and fuel metastasis has remained a key question. Solid evidence supports that micro-invading cells and early DCCs (eDCCs) are detected in BrCa patients diagnosed with lesions pathologically defined as pre-invasive (i.e. ductal carcinoma in situ, DCIS)[3,4]. Early dissemination was also documented in models of pancreatic cancer[5] arguing that this process may be more widespread than thought previously. Another relevant scenario for early dissemination may be metastatic cancer of unknown primary site which is one of the 10 most frequent cancer diagnoses [6,7] and where cancer cells might initially only acquire disseminating capacity to then only grow in secondary organs .This suggests that DCCs may originate long before tumors are detectable or are defined globally as “invasive” by a pathologist. However, the above studies did not identify and functionalize the mechanisms and gene programs that could fuel early dissemination. We follow the early and late DCCs definition provided by Husemann et al. [3] where “early DCCs” (eDCCs) originate at times when patients are thought to carry only *in situ* (e.g. DCIS) lesions and “late DCCs” are derived from invasive tumors.

Anoikis resistance is a trait of metastatic cells needed to negotiate stress imposed by the varying composition of extracellular matrix microenvironments and loss of adhesion in circulation. Interestingly, anoikis resistance is activated at early stages of HER2-driven mammary cancer by inhibiting the p38 kinase, known to also suppress breast tumorigenesis [8-10]. This process is also accompanied by ERK1/2 activation, which positively regulates motility and invasion [11,12], and changes

in the ductal architecture. Importantly, inactivating mutations in the p38 activator MKK4 [13,14] and amplification of the p38 phosphatase PPM1D [9,15] are also frequent in breast cancer, suggesting that different mechanisms might allow for inactivation of p38–induced anoikis among other processes. We hypothesized that inhibition of p38 signaling might allow anoikis resistant HER2+ early cancer cells to acquire motility and invasion programs that enable dissemination to distant organs.

Here we reveal a mechanism of early dissemination where HER2 overexpression results in the activation of Wnt signaling, which contributes to inhibit p38 activation. This results in HER2 signaling inducing an EMT-like program that involves molecules previously observed to regulate mammary gland morphogenesis [10,16,17]. In early HER2^{+} cancer cells p38α/β inhibition further induces the Wnt-driven EMT dramatically stimulating local invasion, intravasation and early dissemination to target organs, as revealed by high-resolution intravital imaging. All these events take place before overt tumors appear and importantly, this mechanism allows MMTV-HER2+ early cancer cells to disseminate. We further found that eDCCs are maintained initially in a non-proliferative state before they can initiate lung metastasis. Our work reveals a previously unrecognized molecular mechanism for early dissemination where morphogenesis programs like those regulated during mammary ductal tree development [10,16,17] may be subverted by HER2 signaling early during cancer progression to foster early dissemination and spawn numerous eDCCs with metastasis-initiating capacity.

RESULTS

Tumorigenic and Metastasis Initiating capacity of early HER2+ cancer cells.

eDCCs can be detected in the bone marrow (BM) during pathologically defined pre-invasive stages of breast cancer (i.e. DCIS) in both patients and in the Balb-C-derived Balb-Neu-T (NeuT active mutant, MMTV-Her2-T **S-Fig1E**) and MMTV-PyMT mouse models of breast cancer [3,4]. Interestingly, it is during this time and not during the time when primary tumors are overt, that dissemination is maximal (see Hosseini et al.). Using the FvB-derived MMTV-HER2(wt) model [10] (**S-**

Fig1E), we detected eDCCs in lungs or BM during stages where gross pathological analysis reveals only early lesions (ADH,DCIS) and no primary tumors are detected. Disseminated cancer cells detected in animals bearing overt tumors were named DCCs because they represent a mixture of eDCCs and those that arrived later. We found that HER2+/CK8/18+ eDCCs are detected in the blood, BM and lungs of 100% of 14-18 weeks old mice, when only early lesions and no tumors are present (**Fig1A-C, S-Fig1A;** note that the time courses of the FvB-derived and BALB/c-derived MMTV-HER2 (Balb-NeuT) models differ). Thus, early dissemination is commonplace in PyMT and ErbB2 models of breast cancer.

To characterize the behavior of DCCs in lungs we detected P-Rb levels, a marker of G1-exit, in HER2+ single cells (1-3 cell clusters) during early (14-18 weeks) or overt primary tumor stages (28 weeks), where a mixture of single DCCs, micro- (3-50 HER2+ cells) and macro-metastasis (>50 HER2+ cells) is observed (**Fig. 1 D&G, S-Fig1B**). In lungs of mice bearing only early lesions we rarely found micro or macrometastasis and eDCCs predominated as single cells or small clusters (2-3 cells, **Fig. 1 D&G, S-Fig1B**). We found that the vast majority of solitary eDCCs (1-3 cells) in lungs during early stages were negative or weakly stained for P-Rb (19% P-Rb^{weak,} 0% P-Rb^{strong}) compared to growing micro and macro-metastases in mice carrying overt lung lesions and primary tumors (80% P-Rb^{strong}) (**Fig1D&G**). In animals with overt tumors solitary DCCs (1-3 cells) became more proliferative as measured by P-Rb fluorescence intensity (**Fig1D, data not shown**) but even lungs bearing proliferative micro- and macro-metastases (28 weeks old) had numerous quiescent P-Rb^{negative} HER2+ DCCs (**Fig1D&G**). We conclude that early DCCs are a population of primarily P-Rb^{negative} cancer cells and that even in animals bearing metastases >50% of single or small groups of DCCs (2-3 cells), which likely are a mixture of early and later arriving DCCs, are non-proliferative or slow cycling.

We next prepared spheres from early stage MMTV-HER2 cells from tissues (**S-Fig1C**) or tumorspheres from overt MMTV-HER2 tumors. After orthotopic injection in nude mouse mammary fat

pads, tumorspheres (~300/site) from overt tumors efficiently formed primary tumors within 4-12 weeks (**Fig 1E**). However, HER2+ mammospheres (~300/site) produced no obvious palpable tumors in this time (**Fig 1E**). Surprisingly, with an incidence of ~21% (n=14), animals injected in the mammary fat pad with HER2+ mammospheres developed lung metastases (overt and micrometastases) (**Fig. 1E-F**). Macro-metastases originating from early cancer cell mammospheres displayed a glandular phenotype but also an undifferentiated morphology (**Fig1F**). Micrometastases also displayed cortical HER2+ staining, confirming that these cells are lineage-derived from MMTV-HER2 cells injected in the fad pads, and were P-Rb^{strong} (**Fig1F**). Further, macro-metastases originating spontaneously in autochthonous MMTV-HER2 mice were also HER2+ and had a similar percentage of P-Rb^{strong} tumor cells to those derived from mammospheres (**Fig1F-G**). Confirming that tumors derived from HER2+ tumorspheres carry disseminating capacity we were able to detect single HER2+ DTCs in mice injected in the fat pad with tumorspheres and that developed tumors. However, we were unable to find macro-metastases within 1-3 months as animals were sacrificed for the large size of the primary tumors (**Fig 1F-G-E, S-Fig1D**). We conclude that early HER2+ mammospheres are efficient at disseminating and can then form metastasis at a ~20% rate (**Fig1E&F**) and that metastases originating from early HER2+ cancer cells contained in the mammospheres once they initiate growth in lungs they proliferate at similar rates as those originating in mice with large primary tumors.

HER2^{+}/E-cad^{lo}/P-p38^{lo} early Cancer Cells are Motile and Invasive.

We published that inhibition of MKK3/6-p38α/β signaling in wt or early stage HER2+ lesions resulted in anoikis resistance and intermixing of myoepithelial and epithelial cells suggestive of motility [10]. Thus, we tested whether the combined loss of p38 signaling and upregulation of HER2 in early cancer cells might activate a disseminating phenotype.

Detection of P-ATF2 (a p38 activity readout - [10]) and E-cadherin (epithelial marker) in HER2+ and HER2-T+ (from Balb-NeuT) tissues at early stages of progression showed great inter-ductal and

intra-ductal heterogeneity of expression (**Fig2A**). We found that E-Cad^{hi} ducts or individual early cancer cells within each duct were more frequently (>60%) P-ATF2^{hi} (**Fig2A**). Accordingly, >85% of HER2^{+} cells were E-cad^{lo} suggesting that HER2^{+} cells are more frequently E-Cad^{lo}/P-ATF2^{lo} (**Fig2B**). Overt MMTV-HER2 tumors (in FvB mice) showed low levels of E-cadherin, P-p38 and P-ATF2, while maintaining high P-ERK1/2 levels (**Fig2D, S-Fig2A**), suggesting that a HER2^{+}/P-p38^{lo}/E-cad^{lo} profile is also present in primary tumors. The HER2^{+}/P-p38^{lo}/E-cad^{lo} profile was present in ~33.8% of the ductal cells (**Fig2**), suggesting that these cells occur heterogeneously through the early cancer lesions. When correlating these markers with HER2 status in human DCIS lesions, an early cancer lesion that is defined as non-invasive, we found that only HER2^{negative} lesions retained both high P-ATF2 levels and organized E-Cadherin junctions (**Fig2C, S-Fig 2B**). In contrast, HER2^{+} DCIS lesions were typically low for all markers (**Fig2C, S-Fig2B**). As in the MMTV-HER2 mouse model (**Fig2A**), the P-p38/P-ATF2^{lo} profile appears to be present also in HER2^{+} invasive breast carcinomas (n=20) where only HER2^{negative} tumors showed very strong nuclear staining for P-p38 and P-ATF2 (**Fig2E and S-Fig2C)**. Thus, the profile discovered in the MMTV-HER2 model is also present in human HER2+ cancer lesions despite the heterogeneity in the human patient population that is thought not to be faithfully recapitulated by the mouse model. HER2 activation inhibited p38 signaling and E-cadherin junction formation, because treatment of HER2-MCF10A cells, which overexpress HER2, with lapatinib (100 nM, 24 hrs) restored E-cadherin junctions and P-ATF2 levels (**Fig2F**). EGFR, expressed in MCF10A cells, does not appear to play a role in E-cadherin and P-p38 downregulation as these cells which are grown in the presence of EGF retain in basal conditions E-cadherin junctions and high p38 activation [10,18]. Thus, lapatinib at these doses does not seem to have noticeable off target effects. HER2-expressing MCF10A or early MMTV-HER2 cells also resisted anoikis in 3D organotypic cultures and formed misshapen lumen-filled acinar structures as reported (**Fig3A&3C**). These aberrant acini showed outward micro-invasion of single cells (**Fig3A, C, D**) rich in f-actin decorated invadopodia, loss of E-cadherin and focalized laminin-V degradation (**Fig3A, C, D**).

Complete loss of E-cadherin signal was also observed in $HER2^+$ microinvading MMTV-HER2 early cancer cells *in vivo* (**Fig3B**). Interestingly, ~80% of microinvading cells were $HER2^+$ and $CK8/18^+$, suggesting that downregulation of E-cadherin does not indicate a complete loss of epithelial identity; only 20% of CK8/18+ microinvading cells were negative for HER2, which might represent a highly migratory subpopulation identified *in vitro* by Hosseini et al (**S-Fig2D**). The downregulation of E-cadherin in $HER2^+$ cells was vigorously stimulated in isolated early HER2+ cancer cells and in the MCF-10A-HER2 model by further forcing an $HER2^+/p38^{lo}$ profile using p38α siRNA or the p38α/β inhibitor (SB203580) (**Fig3C, D** & **Fig4A-B**). In 3D cultures, occasionally we could observe what appeared to be collective invasion and only after p38α/β inhibition (**Fig3C and D**). We conclude that a subpopulation of $HER2^+/E\text{-}cad^{lo}/P\text{-}ATF2^{lo}/P\text{-}p38^{lo}/CK8/18+$ early invasive cancer cells are at early stages of cancer progression and that HER2 signaling actively induces a $P\text{-}p38^{lo}/E\text{-}cad^{lo}$ profile.

Early $HER2^+/P\text{-}p38^{lo}$ cancer cells display characteristics of an EMT.

The loss of E-cadherin junctions led us to test whether a $HER2^+/P\text{-}p38^{lo}$ profile was linked to the partial or total activation of an epithelium to mesenchyme transition program [19]. Treatment of MCF10A-HER2 acini with a p38α/β inhibitor SB203580 or siRNAs targeting p38α or ATF2 (**Figs3-4**), further accentuated the invasive behavior and caused a dramatic loss of E-cadherin junctions (**Fig4A-B**). A similar effect was found in early MMTV-HER2 cells freshly isolated from mice (16 wks) (**Fig4B, S-Fig 1D**). We also found that both genetic and pharmacological inhibition of p38α or p38α/β, respectively reduced membrane-bound β-catenin and increased active-β-catenin (unphosphorylated β-catenin) (**Fig4A-B**). Accordingly, in early stage MMTV-HER2 glands we found ~66% $HER2^+$ cancer cells to be low for membrane localized β-catenin (indicating pathway activation) (**Fig4D, S-Fig 3A**). Activation of β-catenin signaling in $HER2^+$ cells by p38α/β inhibition was confirmed by upregulation of Axin2 mRNA (a canonical target of β-catenin) in MCF10-HER2 cells (**Fig4C**). The intraductal heterogeneity of HER2 overexpression and membrane β-catenin was observed in both MMTV-HER2

and Balb-NeuT models (**Fig4D, S-Fig3A**). In fact, in >70% of early cancer cells that were HER2$^+$ were also low for membrane β-catenin (**Fig4D, S-Fig3A**). Quantification of E-Cadherin expression showed that the vast majority of HER2+ eDCCs (1-5 cell clusters) in lungs were negative for E-cadherin (**Fig4E**). This argues that the loss of E-cadherin possibly activated by an EMT-like program, persists in the single eDCCs (1-3 cell clusters) in lungs (**Fig1**).

Importantly, systemic inhibition of p38α/β for 2 weeks in MMTV-HER2 mice at early stages of progression (14-18 wks old) when no palpable tumors are detectable (**S-Fig 1D**) caused a robust translocation of β-catenin from the membrane to the nucleus and a dramatic loss of E-cadherin junctions in the vast majority of early cancer cells (**Fig5A-B**). Thus, a certain level of p38α/β activity might represses an EMT-like phenotype and prevent HER2$^+$ early cancer cells from disseminating. To confirm this prediction we measured CK8/18+ and/or HER2+ pre-malignant cancer cells in peripheral blood, in BM and lungs of MMTV-HER2 mice carrying early lesions (**Fig5C-E**). We found that a 2 week treatment with SB203580 robustly increased the numbers of CK8/18+ circulating cancer cells. This was followed by an increase in the total number of CK8/18+/HER2$^+$ eDCCs in the BM and HER2$^+$ eDCC in lungs (**Fig5C-E**). The detection of CK8/18 alone or with HER2 in BM eDCCs argues that these are epithelial cells and not leukocytes with ectopic expression of HER2 due to MMTV aberrant activation as reported previously [3]. The median number of eDCCs in the BM compartment is equivalent to ~1.3 eDCCs/ 10^6 BM host cells in control groups and ~8 eDCCs/10^6 BM host cells in SB203580 treated animals. We did find that some eDCCs were CK8/18+ and HER2-negative as found by Hosseini et al. (not shown), suggesting that both subpopulations may be disseminating individually or in a cooperative manner. However, only when considering the HER2$^+$/CK8/18+ early DCCs the stimulation of dissemination by SB203580 was significant; HER2 might enable a more efficient EMT-like response to p38 inhibition (**Fig5C-E**). These data confirm that early HER2$^+$ cancer cells disseminate and can be further stimulated to exit the early lesions by forcing a p38^{lo} profile.

To test the contribution of p38 to the EMT-like behavior independently of HER2, we compared

E-cadherin junctions and membrane/nuclear β-catenin in wild type FvB mice treated with or without SB203580 or wild type MKK3+/+|MKK6+/+ and MKK3−/−|MKK6+/− C57B mice (MKK3 and MKK6 activate all p38 isoforms). We found that in normal wild type tissues, inhibition of the MKK3/MKK6-p38 pathway caused a loss of E-cadherin junctions (**S-Fig3G**), but not nuclear translocation of β-catenin (**S-Fig3H**). Further, the mammary duct architecture was not perturbed despite the loss of E-cadherin junctions because luminal cells expressed CK8/18 and the α-smooth muscle actin positive myoepithelial layer was intact (**S-Fig3H**). We conclude that SB203580 recapitulates the genetic ablation of the MKK3/MKK6-p38 pathway and that this pathway regulates E-Cadherin junction formation (**S-Fig3G**). Further, only in the context of HER2 upregulation does p38 inhibition induce nuclear translocation of β-catenin (**Fig5A-B**).

High-resolution live-cell imaging of early dissemination.

We next used high-resolution intra-vital imaging [20] of MMTV-HER2-CFP transgenic mice to unambiguously record at single-cell level resolution the micro-invasive capacity of early $HER2^+$ invasive cancer cells (**Fig6, S-Fig1E**). To monitor early cancer cell motility before primary tumor development we designed a mammary imaging window to accommodate the depth and lax consistency of the mammary fat pad tissue. 2-photon imaging of a small fraction of the ductal tree in vehicle treated HER2-CFP mice where the vasculature is revealed by i.v. delivered dextran-rhodamine (DR) [20]) showed that early cancer cell motility and local invasion was infrequent at 10 weeks when the ducts in the MMTV-HER2-NDL5-CFP model still display normal ductal architecture (**Fig6A – Supplemental Movie 1)**. However, at 15 and 18 weeks of progression when early lesions are observed (**Supplemental Fig1**), local invasive CFP+ cell translocation and cell motility were detectable even in an imaging area that captures a very small fraction of the transgenic mammary tree (**Fig6A - Supplemental Movies 2 and 3**). At this time we could also detect CFP+ cell translocation and exit from lesions into the stroma (**Fig6A - Supplemental Movies 2 and 3**). Forcing

a HER2^{+}/E-cad^{lo}/P-p38^{lo} profile using a p38α/β inhibitor revealed a strong disruption of the ductal architecture (compare **Fig6A, "normal" architecture, with Fig6B-D and Supplemental Movie 1 with 4**); control ducts at week 12 look similar to those at week 10 in **Fig6A**.

Importantly, p38α/β inhibition revealed at high-resolution active formation of cell protrusions, intra-ductal migration, locomotion along ductal walls and local invasion and intravasation (**Fig6B top and sequence below and Supplemental Movie 4 and 5**). Unlike in 3D cultures (**Fig3C-D**), we did not observe obvious collective cell migration *in vivo* and cells displayed more ameboid-like features that may facilitate invasion [21]. High-resolution imaging and 3D reconstruction of the micro-invasion and intravasation events showed how individual cells micro-invaded outwards from the ductal pre-malignant lesions and invaded through the stroma (**Fig6D - Supplemental Movies 6, 7 and 8**) entering in contact with the blood vessels (**Fig6D - Supplemental Movie 8 and 9**). These high-resolution intra-vital imaging studies unambiguously document early pre-malignant micro-invasion and intravasation.

HER2^{+}/P-p38^{lo} early cancer cells acquire a Wnt^{hi} phenotype.

We next measured the expression of 86 EMT related genes expressed in control (DMSO) and SB203580 treated MCF10A and MCF10A-HER2 acini (**Fig7A**). HER2 expression or p38 inhibition alone induced a shared 14-gene EMT signature (**Fig7A**), suggesting that both kinases operate antagonistically on the same pathway. The signature, (confirmed by subsequent qPCR (**S-Fig3B-C**)), included non-canonical *WNT* ligands (WNT5a/b, WNT11) and a WNT receptor (*FRZD7*), canonical EMT transcription factors (*TWIST, SNAIL, SLUG*) and *ERBB3* and was further upregulated by p38 inhibition in HER2-MCF10A cells (**Fig7A**). Wnt4 (not in our array) was also upregulated in murine early cancer cells (Hosseini et al.) and *E-cadherin* mRNA was downregulated by p38 inhibition in HER2-MCF10A acini (**Fig7B**). *SNAIL* and *TWIST* were also upregulated when HER2-MCF10A 3D cultures were treated with siRNAs targeting *p38*α or *ATF2* (**S-Fig3D**), and systemic treatment of early

MMTV-HER2 mice with SB203580 resulted in an 8-fold upregulation in *TWIST*, mRNA in mammary gland tissues *in vivo* (**Fig7B**). These data suggest that p38 exerts an inhibitory function over HER2 signaling and Wnt-ligand expression in early cancer cells and confirm that *in vivo* p38 signaling restricts the expression (*TWIST)* and/or function (β-catenin) of EMT transcription factors. We conclude that HER2 activation and p38 inhibition cooperate to establish a Wnt signaling-associated EMT, which is sufficient to allow early invasive cancer cells to disseminate.

We next tested if Wnt ligands (**Fig7A and S-Fig3B&C**) were playing a functional role in HER2-driven EMT either alone or in combination with p38 inhibition. When HER2-MCF10A cells were treated with SB203580 the *Axin2* (β-catenin target – canonical Wnt signaling) mRNA was induced and this response was almost completely eliminated in MCF10A-HER2 cells expressing the Wnt-ligand antagonist sFRP (canonical and non-canonical Wnt ligand inhibitor) (**Fig7C, S-Fig3E**). Recombinant soluble Wnt3a produced by L-cells ([22] and methods) also stimulated expression of *Axin2* in HER2-MCF10A cells. Importantly, Wnt3a induction of *Axin2* was significantly inhibited by overexpression of a constitutively active p38α kinase cDNA (**Fig7D**). We conclude that $HER2^{+}/p38^{lo}$ pre-malignant cells rely on Wnt ligands, possibly both canonical and non-canonical, to induce the EMT.

Next, HER2-MCF10A and sFRP expressing HER2-MCF10A cells were treated with or without SB203580 (**Fig7E-F, S-Fig 3E**). Loss of E-cadherin junctions and membrane-localized β-catenin after p38α/β inhibition was blocked in sFRP expressing cells (**Fig7F**). Importantly, the micro-invasion that observed in $HER2^{+}$/P-$p38^{lo}$ colonies after p38 inhibition was blocked by sFRP (**Fig7E-F**) and by the canonical Wnt inhibitor DKK1, which also reversed the E-cadherin loss induced by p38 inhibition (**S-Fig 3F**). Our data and the finding that in the Balb-NeuT model (Hosseini et al.), Wnt4 and RANKL upregulation promote a highly migratory signal in early cancer cells led us to conclude that *via* Wnt signaling HER2 activation in the context of low p38α/β activity results in an EMT-like response.

Collectively these signals allow a previously identifiedbut not characterized[3] sub-population of early invasive cancer cells to disseminate.

DISCUSSION

Previous studies determined that early DCCs occur in the MMTV-HER2 and MMTV-PyMT models and as well as in models of pancreatic cancer and in patients[3-5]. These studies also showed that MMP9 and Twist upregulation appeared to correlate with the early dissemination phenotype, but this was the only descriptive information available and thus the relevance of these markers remained unknown[3]. Our findings now provide a molecular and functional description of the eDCCs by identifying this subpopulation of early invasive cancer cells as $HER2^{+}$/CK8/18+/Wnt^{high}/P-$p38^{low}$/E-cad^{low}. We further show that the eDCC precursors carry an inherent capacity to migrate, intravasate and lodge in secondary organs. Remarkably, these eDCCs show metastasis-initiating capacity. In both our and the Hosseini et al., study, early cancer cells disseminated spontaneously in both MMTV-HER2-wt (FvB-HER2) and –ErbbB2-T (Balb-NeuT) models from autochthonous tissue, fat pad injected mammospheres or from transplanted pre-malignant mammary tissue (Hosseini et al). Husseman et al[3]. also showed that early dissemination also occurs in the MMTV-PyMT mouse model and Stanger and colleagues documented early dissemination in a pancreatic cancer model[5], suggesting it's not a rarity of the HER2 models and that other cancer subtypes can disseminate early. As shown by Hosseini et al., this dissemination seems to be more efficient than that observed in large primary tumors. Majorities of HER2+ eDCCs once in lungs are predominantly negative for P-Rb, a proliferation marker. This suggests that eDCCs can enter a state of dormancy or slow-cycling. As seen following the injection of early HER2+ cancer cell-derived mammospheres into the fat pad of nude mice, eDCCs eventually were able to form HER2+ metastasis in the absence of overt tumors. The exact reasons for this divergence in phenotypes in the primary site are still unclear. However, the

early progressed nature of the early cancer cells is possibly a contributing factor. It is also possible that unlike the lung, the mammary fat pad is not permissive for growth of the early DCCs but is permissive for invasion and dissemination. These results may also shed light into how to model and detect a frequent cancer diagnosis known as metastasis of unknown primary cancer.

The vast majority (~98%) of eDCCs in lungs, which were also single cells or <5 cell clusters, were HER2+ but E-cadherin negative. Only a very small fraction appeared to be able to restore E-cadherin expression and this was observed only in clusters >5 cells. However, the micro-invading cells and a proportion of eDCCs in the bone marrow were CK8/18+, suggesting that a partial EMT program may be sufficient for early dissemination without losing epithelial markers. Dissemination proceeds when collective invasion is activated in CK14+/p63+ basal mammary epithelial cells without evidence of EMT [23]. Also early cancer cell dissemination may follow a basic program of invasion that does not require a full EMT and/or complete E-cadherin downregulation[24]. We argue that when HER2 upregulation is combined with p38 inhibition at least a 14-gene EMT gene module is activated and linked to early dissemination. It is possible that even this partial EMT coupled to other microenvironmental cues[21] causes a disseminating phenotype in early cancer cells. This hypothesis is supported by our recent study (Linde et al., submitted) showing that mammary tissue macrophages (MTMs) are recruited by early HER2+ cancer cells in a CCL2 dependent manner. The recruited MTMs secrete Wnt-1 and further stimulate the HER2-driven EMT-like response.

That p38 signaling prevents the loss of E-cadherin and turning on an EMT-like program is a novel finding. However, how p38 signaling executes these functions is not entirely clear. ATF2 is a likely candidate in activating a program that prevents an EMT as it can block β-catenin activity [25] as *ATF2* RNAi upregulated *TWIST and SNAIL* and a p38α active mutant blocked *AXIN2* induction by Wnt3a. Our data also suggests that if eDCC need to deactivate p38 signaling for dissemination, the non-proliferative or dormant nature of eDCCs in lung might be p38-independent. Thus, the

mechanisms of eDCC dormancy might be different from those reported previously by us in more progressed tumor models[26] and may be in line with those proposed by others[27].

Our data suggest that HER2^{+} cells may aberrantly activate a Wnt-driven program of motility and invasion observed during branching morphogenesis that requires downregulation of p38 signaling and leads to dissemination. Interestingly, Wnt and TGFβ signaling in conjunction with progesterone receptor-B (PgR) favored side branching [16]. With Hosseini et al., we also found that PgR and Wnt4 signaling is enriched in the pre-malignant tissues that spawned eDCCs. As highlighted also by Hosseini et al., wild type ducts that were still undergoing morphogenesis showed also a PgR^{hi}/P-ATF2^{lo} profile. This supports our hypothesis that HER2 co-opts a mechanism of invasion and motility active during morphogenesis[16] and that its deregulation results in early dissemination. Importantly, PgR-signaling is known to induce Wnt4 expression and PgR and HER2 expression overlapped during early stages, but not during overt tumor stages of mammary cancer progression in the MMTV-Neu models. How HER2 and Wnt crosstalk to inhibit p38 is not clear, but HER2 inhibition restored P-ATF2 and E-cadherin levels. However, whether this is WNT-dependent is unclear. One possibility is that HER2, PgR and/or Wnt regulate the expression of p38 phosphatases to turn off this signal[9].

Early stage lesions in adult mice were presumed to be mainly sessile and thus, imaging cell motility during these stages was never attempted. Local invasion and intravasation have been elegantly documented in invasive mammary tumors [28-30]. Our intra-vital imaging now shows that these events are not an exclusive property of advanced tumor cells from overt lesions and that they can be carried out by early cancer cells. These events were originating from the ductal structures, because while MMTV-Cre-mediated recombination can occur outside of mammary tissues [31] we could not detect any CFP cells randomly passing through the imaging fields of any of the imaged mice. Interestingly, local invasion was never observed to be collective as observed in 3D systems, including ours ([23] and **Fig3**).

Our work supports the hypothesis that during long periods of mammary cancer progression, and even during early stages, specific mechanisms drive dissemination of a subpopulation of early cancer cells. This suggests the existence of heterogeneous DCCs arising from all stages of progression, which has not been really taken into account when studying metastasis. This process can produce non-cycling eDCCs, but further analysis is required to determine whether these cells display dormancy characteristics[2]. An important and difficult question to answer is whether and in which ways eDCCs contribute to metastasis. Recent clinical studies showed that 50% of DCIS patients that developed metastasis did so without ever developing any local recurrence[32]. While these metastasis occur at low frequency (~8%[32]) these clinical data supports that eDCCs may be metastatic. This is one possible scenario where our findings might explain how tumors thought not to be metastatic can indeed spread. Another important scenario for which there is no mechanisms or models is metastasis of unknown primary cancer. This diagnosis accounts for 3-5% of all malignancies and ~4.2% of all solid cancer cases/year, of which 50% are adenocarcinomas[6,7]. Thus, the mechanisms we unraveled might be applicable to a broad scope of cases of dissemination without an obvious primary lesion. An additional scenario where understanding early dissemination might be useful was illustrated by a detailed genetic analysis of prostate cancer metastases and primary tumor by Haffner et al[33]. In this study, 7 metastases resected 17 years after radical prostatectomy showed evolutionary traits that could be traced back to a small low-grade subpopulation of cells in the primary tumor, not from the rest of the tumor deemed more “aggressive” by pathology [33]. Thus, early invasive cells in the primary site could disseminate and eventually form metastases that did not evolve in the same way as the rest of the primary tumor clones.

Our work significantly expands upon previous work by Huseman et al.,[3] because now we identify the eDCC and provide mechanisms governing early dissemination that had remained unknown until this point. This study provides novel insight into how a tumor suppressor pathway such as p38, might have previously unrecognized metastasis suppressive function by blocking HER2 and

Wnt signaling and in consequence early dissemination. These findings may have important implications in the treatment of lethal breast cancer metastasis but also other epithelial cancers that go undetected but form metastasis and finally it may expand our understanding of DCC heterogeneity and how to target it.

EXPERIMENTAL PROCEDURES.

See **Supplemental Experimental Procedures** for additional procedures

Cells and cell culture. MCF10A-HER2 cells expressing sFRP were generated using sFRP lentiviral vectors. Wnt3a and DKK1 conditioned media was prepared from Wnt3a expressing L-cells and Dkk1 expressing 293T cells. Vectors and sFRP plasmids were a kind gift from Dr. Stuart Aaronson, ISMMS, New York, NY. Conditioned media was prepared from cells cultured with serum free medium (DMEM + 1%P/S) for 24 hours and then concentrated using Vivaspin 20 Centrifugal Concentrating tubes (Sartorius, VS2021) at 3000g up to 3 hours until desired concentration (10x) was reached.

Mammospheres and tumorspheres assays. Animal procedures were approved by the Institutional Animal Care and Use Committee (IACUC) of Icahn School of Medicine at Mount Sinai protocol 08-0366. MMTV-HER2 mice were sacrificed using CO_2 at age 14-18wk or when overt tumors had formed (PT). For mammosphere preparations, all 5 pairs of glands in mice were checked for the presence of any visible small lesions or palpable tumors when processed for early cancer cell and none were found. Even when other mammary glands were inspected microscopically in whole mounts we could not detect small tumors. Whole mammary glands or tumors were digested in Collagenase/BSA at 37°C for 45-60min. Red blood cell lysis buffer was used to remove blood cells from cultures and cells were then plated for 10-15min in DMEM+10%FBS in 35mm dishes at 37°C to for fibroblast removal. Cells were then incubated in PBS-EDTA 2mM for 15min at 37°C and passed through a 25 gauge needle. Cell suspensions were then filtered through a 70μM filter before counting. Cells were seeded

in 6-well ultra low adhesion plates at a density >5.0x10^5 cells per well in 1mL mammosphere media (DMEM/F12 (Gibco 11320-082), 1:50 B27 (Invitrogen 17504-044), EGF (Peprotech AF-100-15-A), 1:100 Pen/Strep). Approximately 300 spheres were injected per site. Suspension cultures were spun at 300rpm for 4min and then suspended in 150ul PBS++/300 spheres. Matrigel (Corning 356231) was then added in a 1:1 ratio. Spheres were injected into the two 4^{th} inguinal gland fat pad using a 27-gauge needle.

3D mammary primary epithelial cell cultures. MMTV-HER2 mice were sacrificed using CO_2 at age 14-18wk and MECs were isolated using the same protocol used for mammosphere preparation.). Similar to mammosphere preparations, all 5 pairs of glands in mice were checked for the presence of any visible or palpable tumors when processed for early cancer cell and none were found even in whole mounts prepared from mammary glands from the same mouse processed for mammoprsphere preparation. 5.0X10^4 MECs were seeded in in 400ul Assay Medium in 8-well chamber slides with 40ul of Matrigel. Acini formed at an efficiency of around 30 acini/1.0x10^4 MECs plated. Cultures were treated every 24 hours with 5uM DMSO/SB203580 and 500ng/ml DKK1 for 48 hours following acini formation and fixed for immunofluorescence (IF) with 4%PFA or 10% Formalin with phosphatase and protease inhibitors.

Patient samples. Paraffin embedded sections from DCIS and invasive breast cancer patient tumors were obtained from the Cancer Biorepository at Icahn School of Medicine at Mount Sinai, New York, NY. Samples were de-identified and obtained with Institutional Review Board approval, which indicated that this work does not meet the definition of human subject research according to the 45 CFR 46 and the Office of Human Subject Research. IF and immunohistochemistry (IHC) analysis was done using samples from 10 DCIS and 20 invasive breast cancer patients. Invasive breast cancer samples included Luminal A, B and HER2 positive subtypes.

Circulating Cancer Cells (CCCs) and Disseminated Cancer Cells (DCCs) detection. 16 week-old MMTV-HER2 mice were treated with SB (10 mg/kg) or DMSO for 2 weeks and blood was drawn by cardiac puncture following IACUC protocols. CCCs were purified using negative lineage cell-depletion kit (Cat 130-090-858, Milteny) fixed and stained with anti-CK8/18 antibody in cytospin preparations. Bone marrow cells from 4 long bones were flushed out Minimum Essential Medium Eagle (MEME) (Sigma, MO, USA) using 26-G needle and 1 ml syringe. Tumor cells were enriched by Ficoll-Paque plus (GE Healthcare) density gradient separation and filtered through 30uM nylon mesh to remove large aggregates. Cells were fixed with 3% PFA for 20 min on ice and cytospin preparations were carried out by centrifugation of bone marrow cells at 500 rpm for 3 min using poly-L-lysine-coated slides (Sigma, MO, USA). DCCs were stained with anti-CK8/18 or anti-HER2 antibodies in cytospin preparations were analyzed. We screened 0.5-2.0x10^6 BM cells, which represents 20% of the total BM cells per mouse and then normalized to 1x10^6 BM cells. Similar to mammosphere preparations, all 5 pairs of glands in mice were checked for the presence of any visible or palpable tumors when processed for early cancer cell and none were found as described above.

Intra-vital microscopy. Imaging of 3D acini was done using confocal microscopy. Images were obtained using Leica Software on a Leica SP5 confocal microscope. Mammary gland section imaging was done using Leica DM 550 fluorescence microscope using Leica Software. Dye Separation analysis was done using Leica Software. 2-photon imaging was performed following the reported protocols [20]. Intravital imaging was performed using a custom-built two-laser multiphoton microscope following previously reported imaging protocols[20]. All procedures were conducted in accordance with the National Institutes of Health regulations and approved by the Albert Einstein College of Medicine animal use committee. More detailed description of two-photon imaging can be found in Supplemental Experimental Procedures.

Statistical Analysis. Statistical Analysis was done using Prism Software. Differences were considered significant if *P* values was <0.05. For all cell cultures, one tailed *student t-tests* were performed. For mouse experiments one tailed *Mann-Whitney* tests were used.

AUTHORS CONTRIBUTIONS. KH: designed, optimized and performed experiments, analyzed data and co-wrote the manuscript, MSS: designed and optimized experimental approach, performed experiments, designed and executed intravital imaging experiments, provided guidance and oversight, analyzed data and co-wrote the manuscript, HH: designed and performed experiments and analyzed data, AAV: performed experiments, CN: provided human histological samples and provided histopathological analysis, RD: provided mouse mammary gland samples, CK: designed experiments, analyzed data and co-wrote the manuscript, DE: designed and executed intravital imaging, analyzed data and co-wrote the manuscript. JC: designed intra-vital experiments, analyzed data and co-wrote the manuscript, EFF: provided expertise in the MMTV-HER2 model, deigned experiments and analyzed data, JAA-G: designed and optimized experimental approach, provided general guidance and oversight, analyzed data and co-wrote the manuscript.

Acknowledgements. We thank the Aguirre-Ghiso, Klein and Condeelis labs for useful discussions. Grant Support: Samuel Waxman Cancer Research Foundation Tumor Dormancy Program to J.A.A-G. and E.F.F., NIH/NCI (CA109182) to J.A.A-G., NCI - Tumor Microenvironment Network (CA163131) to J.A.A-G and J.C., NIH/NCI F31 CA183185 to K.H., DoD-BCRP Breakthrough Award (BC132674) to J.A.A-G and J.C., DoD-BCRP Grant (BC112380) to M.S.S.

REFERENCES:

1 Klein, C. A. Framework models of tumor dormancy from patient-derived observations. *Current opinion in genetics & development* (2010).

2 Sosa, M. S., Bragado, P. & Aguirre-Ghiso, J. A. Mechanisms of disseminated cancer cell dormancy: an awakening field. *Nature reviews. Cancer* **14**, 611-622, doi:10.1038/nrc3793 (2014).

3 Husemann, Y. *et al.* Systemic spread is an early step in breast cancer. *Cancer Cell* **13**, 58-68, doi:10.1016/j.ccr.2007.12.003 (2008).
4 Schardt, J. A. *et al.* Genomic analysis of single cytokeratin-positive cells from bone marrow reveals early mutational events in breast cancer. *Cancer Cell* **8**, 227-239, doi:10.1016/j.ccr.2005.08.003 (2005).
5 Rhim, A. D. *et al.* EMT and dissemination precede pancreatic tumor formation. *Cell* **148**, 349-361, doi:10.1016/j.cell.2011.11.025 (2012).
6 Pavlidis, N., Briasoulis, E., Hainsworth, J. & Greco, F. A. Diagnostic and therapeutic management of cancer of an unknown primary. *European journal of cancer* **39**, 1990-2005 (2003).
7 Pavlidis, N. & Fizazi, K. Carcinoma of unknown primary (CUP). *Critical reviews in oncology/hematology* **69**, 271-278, doi:10.1016/j.critrevonc.2008.09.005 (2009).
8 Ventura, J. J. *et al.* p38alpha MAP kinase is essential in lung stem and progenitor cell proliferation and differentiation. *Nature genetics* **39**, 750-758 (2007).
9 Bulavin, D. V. *et al.* Amplification of PPM1D in human tumors abrogates p53 tumor-suppressor activity. *Nature genetics* **31**, 210-215 (2002).
10 Wen, H. C. *et al.* p38alpha Signaling Induces Anoikis and Lumen Formation During Mammary Morphogenesis. *Science signaling* **4**, ra34, doi:10.1126/scisignal.2001684 (2011).
11 Pearson, G. W. & Hunter, T. Real-time imaging reveals that noninvasive mammary epithelial acini can contain motile cells. *The Journal of cell biology* **179**, 1555-1567 (2007).
12 Klemke, R. L. *et al.* Regulation of cell motility by mitogen-activated protein kinase. *The Journal of cell biology* **137**, 481-492 (1997).
13 Su, G. H., Song, J. J., Repasky, E. A., Schutte, M. & Kern, S. E. Mutation rate of MAP2K4/MKK4 in breast carcinoma. *Human mutation* **19**, 81, doi:10.1002/humu.9002 (2002).
14 Teng, D. H. *et al.* Human mitogen-activated protein kinase kinase 4 as a candidate tumor suppressor. *Cancer Res* **57**, 4177-4182 (1997).
15 Bulavin, D. V. *et al.* Inactivation of the Wip1 phosphatase inhibits mammary tumorigenesis through p38 MAPK-mediated activation of the p16(Ink4a)-p19(Arf) pathway. *Nature genetics* **36**, 343-350 (2004).
16 Brisken, C. *et al.* Essential function of Wnt-4 in mammary gland development downstream of progesterone signaling. *Genes Dev* **14**, 650-654 (2000).
17 Nelson, C. M., Vanduijn, M. M., Inman, J. L., Fletcher, D. A. & Bissell, M. J. Tissue geometry determines sites of mammary branching morphogenesis in organotypic cultures. *Science* **314**, 298-300, doi:10.1126/science.1131000 (2006).
18 Debnath, J. *et al.* The role of apoptosis in creating and maintaining luminal space within normal and oncogene-expressing mammary acini. *Cell* **111**, 29-40 (2002).
19 Thiery, J. P., Acloque, H., Huang, R. Y. & Nieto, M. A. Epithelial-mesenchymal transitions in development and disease. *Cell* **139**, 871-890 (2009).
20 Entenberg, D. *et al.* Setup and use of a two-laser multiphoton microscope for multichannel intravital fluorescence imaging. *Nature protocols* **6**, 1500-1520, doi:10.1038/nprot.2011.376 (2011).
21 Liu, Y. J. *et al.* Confinement and low adhesion induce fast amoeboid migration of slow mesenchymal cells. *Cell* **160**, 659-672, doi:10.1016/j.cell.2015.01.007 (2015).
22 Grumolato, L. *et al.* Canonical and noncanonical Wnts use a common mechanism to activate completely unrelated coreceptors. *Genes Dev* **24**, 2517-2530, doi:10.1101/gad.1957710 (2010).
23 Cheung, K. J., Gabrielson, E., Werb, Z. & Ewald, A. J. Collective invasion in breast cancer requires a conserved basal epithelial program. *Cell* **155**, 1639-1651, doi:10.1016/j.cell.2013.11.029 (2013).

24 Shamir, E. R. *et al.* Twist1-induced dissemination preserves epithelial identity and requires E-cadherin. *The Journal of cell biology* **204**, 839-856, doi:10.1083/jcb.201306088 (2014).
25 Bhoumik, A. *et al.* Suppressor role of activating transcription factor 2 (ATF2) in skin cancer. *Proc Natl Acad Sci U S A* **105**, 1674-1679 (2008).
26 Bragado, P. *et al.* TGF-beta2 dictates disseminated tumour cell fate in target organs through TGF-beta-RIII and p38alpha/beta signalling. *Nat Cell Biol* **15**, 1351-1361, doi:10.1038/ncb2861 (2013).
27 Brabletz, T. To differentiate or not--routes towards metastasis. *Nature reviews. Cancer* **12**, 425-436, doi:10.1038/nrc3265 (2012).
28 Dovas, A. *et al.* Visualization of actin polymerization in invasive structures of macrophages and carcinoma cells using photoconvertible beta-actin-Dendra2 fusion proteins. *PloS one* **6**, e16485, doi:10.1371/journal.pone.0016485 (2011).
29 Oser, M. *et al.* Cortactin regulates cofilin and N-WASp activities to control the stages of invadopodium assembly and maturation. *The Journal of cell biology* **186**, 571-587, doi:10.1083/jcb.200812176 (2009).
30 Lorenz, M., Yamaguchi, H., Wang, Y., Singer, R. H. & Condeelis, J. Imaging sites of N-wasp activity in lamellipodia and invadopodia of carcinoma cells. *Current biology : CB* **14**, 697-703, doi:10.1016/j.cub.2004.04.008 (2004).
31 Wagner, K. U. *et al.* Spatial and temporal expression of the Cre gene under the control of the MMTV-LTR in different lines of transgenic mice. *Transgenic research* **10**, 545-553 (2001).
32 Narod, S. A., Iqbal, J., Giannakeas, V., Sopik, V. & Sun, P. Breast Cancer Mortality After a Diagnosis of Ductal Carcinoma In Situ. *JAMA oncology* **1**, 888-896, doi:10.1001/jamaoncol.2015.2510 (2015).
33 Haffner, M. C. *et al.* Tracking the clonal origin of lethal prostate cancer. *The Journal of clinical investigation* **123**, 4918-4922, doi:10.1172/JCI70354 (2013).

FIGURE LEGENDS:

Figure 1: HER2+ cancer cells disseminate early and form metastasis. (A) Circulating cancer cells (CCCs) were isolated from blood of HER2 mice at early stages of cancer progression (age 14-18wk) and cytospin preparations were stained for the epithelial marker CK8/18 (green) and nuclei with DAPI (blue). # CTCs/mL blood in mice can be found in **S-Fig 1**. Scale bar=10μM **(B)** IHC for HER2 on lung sections from MMTV-HER2 mice (age 14-18wk) was used to detect early disseminated cancer cells (DCC) within the lung (scale bar=25μM). Regions (i and ii) are augmented in the panel images (right). Empty arrowheads indicate HER2+ DTCs and filled arrowheads point to host HER2- cells within the lung (scale bar=10μM). Number of HER2+ DTCs/field can be found in **S-Fig1**. **(C)** Disseminated cancer cells (DCCs) in the bone marrow of MMTV-HER2 mice were extracted from four hind limb long bones (age 14-18wk). DCCs were detected in cytospin preparations of whole bone marrow samples by staining for the epithelial marker CK8/18 (green), HER2 (red) and nuclei with DAPI (blue).

Cells, which were CK8/18+, HER2+ or +/+ were considered eDCCs. The total # of eDCCs/bone marrow can be found in **S-Fig1**. Right panels show individual channel signals and the merged channels are shown on the left detecting a BM CK8/18+/HER2+ DTC (empty arrowhead) next to a CK8/18-/HER2- bone marrow cell (full arrowhead). Scale bar=10μM. **(D)** IF using antibodies for HER2 (red/yellow) to detect DTCs, p-Rb (green) as a marker of proliferation, and DAPI (blue) for nuclei in lung sections from MMTV-HER2 mice at early stages of progression (age 14-18wks) and mice with overt tumors (age 25wk and up). Early DCCs (eDCC) were detected in 14-18wk MMTV-HER2 mice (middle and right top panels). IgG control for HER2 in **S-Fig 1**. Lungs carrying a mixture of early and late (e/L) DCCs found in mice bearing overt tumors (bottom middle and right panels). *Lower two panels*, Tumor (right) and metastases (left) sections stained for HER2 (red) and p-Rb (green). Scale bars=10μM. **(E)** Table showing the tumorigenic and metastatic efficiency of sphere cultures prepared from MMTV-HER2 mice and injected into nude mice as outlined in **S-Fig 1**. Primary tumor incidence (PT) as well as lung macro-metastases (Mets) in these mice was monitored up to one year. Tumorsphere injected mice were sacrificed by 3 months due to large tumor size with no detectable lung macro-metastases. Mammosphere injected mice were tracked up to a year with no primary tumor incidence while 3/14 mice had detectable lung macro-metastases. **(F)** H&E staining for sections of lung metastasis found in nude mice injected with MMTV-HER2 mammospheres (*upper left*). *Upper right*, shows differentiated glandular ductal structures found within the same metastasis. *Bottom panel*, representative image of P-Rb levels (green) and HER2 (red) staining in a micro-metastasis from mammosphere injection. Scale bar=10μM (top right, bottom image), 100 μM (top left image). **(G)** The % of P-Rb positive HER2-DTCs was quantified in mice with early lesions (E) overt tumors (E/L) (n>200cells). Single DTCs were considered when $\leq$3 HER2+ DTCs were found solitary or a cluster (2-3 HER2+cells). The % of p-Rb cells within metastases was also quantified in HER2 mice carrying over tumors as shown in **Fig 1D** (Met) (n=5 metastasis) or in metastases initiated from injection of MMTV-HER2 mammospheres as seen in **Fig 1F** (n=11 micro, n=4 macro). Micro-

metastases were considered as clusters ranging from 3-20 cells. Macro-metastases were clusters >20 cells. Values = mean % p-Rb + cells with error bars representing ± SEM. *=p<0.05

Figure 2: E-cadherin, HER2 and p38 activation in early and invasive breast cancer cells. (A) Early stage MMTV-HER2 mammary gland sections (age 14-18wk) co-stained for E-cadherin (green) and p-ATF2 (red). Representative images of E-cad^{hi}/p-ATF2^{hi} (TOP) and E-cad^{LOW}/p-ATF2^{LOW} (BOTTOM) ducts in MMTV-HER2 mammary ducts are shown (scale bar=25μM). Middle four panels, heterogeneity for E-cad and P-ATF2 signals: P-ATF2^{HIGH}/E-cad^{HIGH} cells (left column) and p-ATF2^{LOW}/E-cad^{LOW} cells (right column) in the MMTV-HER2 and MMTV-HER2-T (Balb-Neu-T, 15 weeks old) models (scale bar=10μM). Empty arrows highlight examples of P-ATF2^{HIGH}/E-cad^{HIGH} cells within a duct. Full arrows point to p-ATF2^{LOW}/E-cad^{LOW} cells (scale bars=10 μM). *Left graph*, the heterogeneity for P-ATF2 and E-cadherin signals was quantified by determining the percent of E-cad^{HI} cells/duct that were P-ATF2$^{HI/LO}$. Values represent mean with errors bars representing SEM. (HER2 n=30 ducts; HER2-T n=10 ducts). **(B)** Top and bottom panels, early stage MMTV-HER2 mammary glands co-stained for E-cadherin (green), HER2 (red) and DAPI (blue). Empty arrows indicate HER2^{HIGH}/E-cad^{LOW} cells and full arrows indicate HER2^{LOW}/E-cad^{HIGH} cells. Bottom panel further illustrates the inter-ductal heterogeneity of E-cadherin and HER2. Inset in bottom panel shows detailed image of boxed region. (Scale bar=10 μM inset, 25 μM panels). Graph shows the percentage of HER2^{HIGH} cells that were E-cadherin$^{LOW/HIGH}$ (n=20 ducts, 2 mice). **(C)** Representative images of DCIS patient samples parallel sections stained for p-ATF2 (Red) HER2 (Green – insets lower row), E-cadherin (green – also insets upper row). Patients were categorized as HER2 positive or negative by IF for HER2 (insets lower row, green). Inset images show detail of E-cadherin junctions in HER2+ and HER2- patients with the empty arrows indicating strong E-cadherin junctions and a full arrow highlighting weak E-cadherin staining. (Scale bars=25μM, 10 μM for inset). Metamorph software was used to quantify HER2, E-cadherin and p-ATF2 fluorescence signal intensity in DCIS samples. Mean

fluorescence intensity (m.f.i)/cell/field in HER2+ (black bars) vs. HER2- (grey bars) patients is represented in the graph (right) with error bars representing SEM values. (n=10 patients) **(D)** MCF10A-HER2 MECs were treated in culture with 100nM Lapatinib or DMSO for 24 hours. Representative images are shown of IF staining for P-ATF2 (Red) and E-cadherin (Green) (Scale bars= 10μM). Quantification of the percent (%) of P-ATF2 positive cells in Lapatinib treated cultures compared to DMSO controls is shown in the graph (right). Boxplot showing median and range (n=300 cells/treatment, 3 biological replicates) *=p<0.05 , **=p<0.01, ***=p<0.0001. **(E)** Cartoon depicting the two subpopulations of cells found at early stages of progression. Bright red cells represent Her2+ cells found at a rate of 42.8±10.84% of cells/duct (n=3 mice, 6 ducts/mouse) multiplied by the frequency at which $Her2^{HI}$ cells are also E-cadherin low (79.2%) we find that ~33.8% of cells within each duct carry a $Her2^{HI}$/$E\text{-}cad^{LOW}$/$p38^{LOW}$ profile. Bright green cells highlight Her2- $E\text{-}cad^{hi}$ cell profiles. Blue coloring was used to provide focus on and clarity on the identified populations but these occur heterogeneously throughthe ductal lesions at the rats described above.

Figure 3: $HER2^{+}$ early cancer cells are $E\text{-}cadherin^{LOW}$ and micro-invasive. (A) MCF10A-HER2 cells cultured in 3D Matrigel were stained for E-cadherin (green) and DAPI (blue). A representative image of acini, left panel (Scale bar=25 μM). Details of $E\text{-}cad^{lo}$ cells microinvading are shown to the right (top and bottom). Empty arrows indicate $E\text{-}cad^{lo}$ cells invading outward from colonies (Scale bar=10 μM). Around 40% of MCF10A-HER2 acini show outward invasion of one cell/colony in equatorial sections (**Fig 3D**). 92±8.3% of outward invading cells were $E\text{-}cadherin^{LOW}$ (n= 20 acini). **(B)** Ealry MMTV-HER2 mammary gland sections (age 14-18wk) co-stained for E-cadherin (green), HER2 (red) and DAPI (blue). Empty arrows indicate $HER2^{+}$/$E\text{-}cad^{LOW}$ cells invading into stroma or out from epithelial layers in ducts. The percent (%) of outward invading cells, which were $E\text{-}cad^{LOW}$ is shown. (n=54-63 cells/mammary gland section, 2 mice) **(C)** MMTV-HER2 MECs were isolated from the mammary glands of 14-18 weeks-old mice before mice had developed tumors. Following formation of

acinar-like structures cultures were treated for 48hr with DMSO or 5μM of the p38α/β inhibitor SB203580. Zoomed regions on the right show the presence of invasive cells only found in SB203580-treated cultures. MMTV-HER2 3D cultures were stained for F-actin (red), Laminin V (green) and DAPI (blue). Empty arrows highlight invasive events; a full arrow indicates intact laminin-V layer in DMSO controls. Quantification of the number of acini with outward invasion in DMSO (C) and SB203580 treated cultures is shown in the graph to the right (DMSO=11; SB=9). Scale bars=25μM **(D)** MCF10A-HER2 cells were seeded in 3D Matrigel and treated for 6 days with the p38 inhibitor SB203580 following acini formation (day 4). Representative images of acini stained for f-actin (red) and Laminin-V (green). Quantification of the percent (%) of acini with outward invasion is shown with error bars representing the SEM. (n=109 acini DMSO, 87 acini SB203580) ***=p<0.001

Figure 4: p38 inhibition promotes EMT markers in HER2+ early cancer cells. (A) MCF10A-HER2 and early MMTV-HER2 MECs were cultured in 3D Matrigel and treated for 6 days and 48 hrs, respectively with the p38α/β inhibitor SB203580 following acini formation. Acini were stained for E-cadherin and β-catenin. Gray scale images in the right MMTV-HER2 panel show magnification of MMTV-HER2 acini for a more detailed view of membrane localized β-catenin. Top right graph panel, shows the quantification of E-cad^{HIGH} and β-cat^{MEM} acini: % E-cadherin is on the left axis (green bars) and %β-catenin in the membrane is on the right axis (red bars). (MCF10A-HER2 n=20acini/treatment, MMTV-HER2 n=10 acini/treatment) scale bars=25μM **(B)** Effect of genetic inhibition of p38α signaling on E-cadherin and β-catenin-based junctions. MCF10A-HER2 (*Left panels*) and MMTV-HER2 cells (*Middle panels)* were cultured in 3D Matrigel and treated as in **A** but with siRNAs targeting p38α as well as a non-targeting control (siCTL). Results were similar to what was seen with the pharmacological inhibitor, SB203580. Quantification of E-cad^{HIGH} and β-cat^{MEM} is shown in the right bottom graph panel in **A** (MCF10A-HER2 n=20 acini/treatment, MMTV-HER2 E-cadherin=30 acini/treatment, b-catenin=10 acini/treatment). Acini were also stained in one trial with an antibody

recognizing the active conformation of β-catenin (see methods). Quantification of acini, which were strongly stained with this antibody, is shown in the top right panel (n=10 acini/treatment). scale bars=25μM **(C)** AXIN2 mRNA levels were measured in MCF10A-HER2 monolayer cultures treated for 24 hours with DMSO control (C) or SB203580 (SB, 5μM). Samples were run in triplicate and values were normalized to GAPDH and fold change over control was determined for five biological replicates. **(D)** Early stage MMTV-HER2 (age 14-18 week) and MMTV-HER2-T (Balb-NeuT age 15 week) mammary gland sections stained for HER2 and β-catenin. Left and right panels show two separate duct examples. Full arrows indicate $HER2^{+}$/β-$catenin^{MEM\text{-}LOW}$ MECs found within the duct while empty arrows highlight $HER2^{-}$/β-$catenin^{MEM\text{-}HIGH}$ MECs (Scale bars=25 μM). The percent (%) of β-$catenin^{MEM\text{-}HIGH}$ and $HER2^{+/-}$ cells per duct was quantified in HER2 and HER2-T and shown in **S-Fig4**. Digital dye separation Leica software module was used on the images. **(E)** Lung sections from MMTV-HER2 mice (age16-20 wks) carrying only early DCCs were stained for HER2 (red), E-cadherin (green) and DAPI (blue) to detect E-cadherin levels in HER2+ DTCs. 98 $\pm$ 0.57% of HER2+ DTCs were E-cadherin negative ($n \geq 100$ DTCs, 3 mice). Scale bar=10 μM, *=$p<0.05$

Figure 5: Effect of p38 inhibition on EMT markers and early dissemination of HER2+ cancer cells *in vivo*. (A-B) Mammary glands from early stage MMTV-HER2 mice treated for 2 weeks with the p38α/β inhibitor SB203580 (age 16-18 weeks, 10mg/kg, i.p every 48hr) were stained for E-cadherin (**A**) and β-catenin (**B**). Boxed areas are magnified in the lower row (Scale bars=10 μM). Empty arrows indicate strong membrane localized β-catenin and full arrows indicate nuclear events in SB203580 mice (Scale bar=10 μM). Quantification of the average % of E-cad^{HIGH} ducts in DMSO (C) and SB203580 treated mice and % of nuclear events/duct is shown in the bottom graph (n=4 mice). **(C)** Whole blood was extracted post-euthanasia from MMTV-HER2 mice (age 14-18wk) treated for two weeks with DMSO (C) or the p38α/β inhibitor SB203580. CCCs were detected as CK8/18+ as in **Fig 1A** and plotted in the graph. Following SB203580 treatment the number of CCCs significantly

increased in MMTV-HER2 mice (n=5 mice). **(D)** Bone marrow samples were collected from two tibias and two femurs of mice treated with DMSO (C) or the p38α/β inhibitor SB203580 as in **A**. Early DCCs that were CK8/18+ and HER2+ or co-stained for both markers in cytospin preparations were quantified and the # of DTC in whole bone marrow is shown in the graph. SB203580 treatment resulted in a significant increase of bone marrow eDCCs (n=5mice/group). The median # of eDCCs in this BM compartment is comparable to ~1.3 eDCCs/ 10^6 BM host cells in control groups and ~8 eDCCs/10^6 BM host cells in SB203580 treated animals. **(E)** DCCs were detected in the lung of early MMTV-HER2 mice treated with DMSO (C) or the p38α/β inhibitor SB203580 as in **Fig 1B**. The number of HER2+ DCCs/field is shown for both DMSO (C) and SB203580 treated mice (n=30 fields, 3 mice/treatment). *p<0.05, **=p<0.01 **(F)** Cartoon depicting the profiles of eDCCs. Her2+/CK18/18+ early cancer cells (RED) are characterized by a Wnt^{HIGH}/EMT^{HIGH}/$p38^{LOW}$ signature and disseminate via the blood to bone marrow and lungs. ~77.4% of micro-invading cells (RED) were characterized by Her2+/CK8/18+ E-cad^{LOW} profile in MMTV-Neu early cancer lesions. Within the lung Her2+/E-cad^{LOW}/pRb^{LOW} cells could be detected in ~78.4% of Her2+ eDTCs.

Figure 6: High resolution 2-photon intra-vital imaging of early dissemination. (A) Stills from intra-vital movies of 10 (left, S-Movie 1), 15 (middle, S-Movie 2) and 18 (right, S-Movie 3) weeks old mammary glands of MMTV-HER2-CFP mice. Blue-white signal pinpoints the CFP+ cells while rhodamine-dextran injected i.v. highlights the vasculature. No events of micro-invasion were observed at 10 wks, while at 15 and 18 weeks micro-invasion and motility were evident. Inset in the left panel shows a detail of a CFP+ duct. The arrows and outlines in the middle 15 wks panel shows CFP+ cells actively microinvading and translocating. Sequence inset in the right 18 wks panel shows active microinvasion and travel of a early cancer cells. Dotted arrow= director of movement. **(B)** Stills from intra-vital movies of a duct from an MMTV-HER2-CFP mice treated with SB203580 for 2 weeks as in Fig5A (S-Movie 4). Note the disorganized ductal structure compared to A and in the inset CFP+ early

cancer cells displaying invadopodia like projections towards the blood vessel. The full arrow in B points to a blood vessel where an intravasation event was filmed and a sequence is shown in the images that span below B and C (S-Movie 5). Dotted line direction of movement and full arrow point out the CFP+ intravasating cell. **(C)** Low power intra-vital still from movie of a early stage duct of MMTV-HER2-CFP mice treated with SB203580 for 4 weeks where events of micro-invasion (full arrows and S-Movie 6) and intravasation are observed (S-Movie 6 and 7). **(D)** *Top panel, h*igh power high resolution intra-vital still from a movie of the area boxed in C showing active breaching of MMTV-HER2-CFP cells from the ductal structure into the stroma and interacting with blood vessels (red) (S-Movie 8). *Middle and bottom panels*, frames of a 3D computer generated reconstruction of the movie in D, top panel (S-Movie 8). The middle panel shows the same projection and the bottom panel a rotated projection to show the interaction (yellow) between early cancer cells (CFP) and blood vessels (red) (S-Movie 9).

Figure 7: HER2 and p38 regulate a Wnt-driven EMT-like program in early cancer cells. (A) MCF10A and MCF10A-HER2 cells were plated in 3D Matrigel and treated from day 6-12 with the p38α/β inhibitor SB203580 (5μM). Gene expression profiling for 86 EMT target genes was performed as described in Experimental Procedures. A 14-gene EMT signature (right gene list) was generated from genes upregulated > 2 fold over three trials and plotted using Gene-E. Green columns represent control values set to 1 and fold change over control is shown in red for each gene. **(B)** Q-PCR array measurement of *E-Cadherin* mRNA levels in MCF10A-HER2 acini treated for 6 days with SB203580 (5μM) and sip38α (20nM). Samples were run in triplicate and normalized to GAPDH. Fold change over control is shown. DMSO was used as a control for SB203580 samples and, non-targeting siRNA was used as a control for sip38α. *Twist* mRNA levels were measured in RNA extracted from early MMTV-HER2 mammary glands (age 14-18wk) treated for 2 weeks with vehicle or SB203580 (10mg/kg, i.p every 48hr). Fold change over control (DMSO) is shown with values normalized to

GAPDH (n=3 mice/treatment); left Y-axis for E-cadherin and right Y-axis for Twist. **(C)** MCF10A-HER2 and MCF10A-HER2-sFRP cells were treated with SB203580 (5uM) for 24hr. *Axin2* mRNA levels were measured with samples run in triplicate using GAPDH as control. Fold change over control is shown with error bars representing SEM for six biological replicates. **(D)** MCF10A monolayer cultures transfected with pcDNA3 (empty vector) and CAp38α (D176A/F372S, constitutively active mutant) plasmids were treated with Wnt3a conditioned media. *Axin2* mRNA levels were measured following 24 hr of treatment. Fold change over control is shown; error bars=SEM for three biological replicates. **(E)** HER2 and MCF10A-HER2-sFRP cells were cultured in 3D Matrigel and treated from Day 6-12 with DMSO or the p38α/β inhibitor SB203580 (5 μM). The number of acini with outward invading cells was quantified and shown in the graph (n=20 acini/treatment, 2 biological replicates) **(F)** MCF10A-HER2 and MCF10A-HER2-sFRP cells were cultured in 3D Matrigel and treated from days 6-12 with SB203580 (5uM). First and second rows from top panels show representative images of IF staining for E-cadherin (green) and the third and fourth rows show β-catenin (red). Insets in the b-catenin images below (F1-F4) show boxed regions in higher detail in the fifth row from top to show disruption of β-catenin junctions. Note the rescue of both E-cadherin and β-catenin^{MEM} in sFRP expressing MCF10A-HER2 acini treated with SB203580. Percent of E-cadherin^{HIGH} and β-catenin^{MEM} acini is shown (mean$\pm$SEM; n=20 acini/treatment, 2 biological replicates). scale bars=25μM *=$p<0.05$. **(G)** Cartoon depicting how early Her2+/CK8/18+ E-cad^{LOW} /P-p38lo disseminating cells (RED) turn on Wnt signaling and inhibit p38 signaling to maintain the EMT-like program. The low or negative levels of HER2 in the non-microinvading cells (GREEN) maintain E-cadherin junctions and p38 activity preventing the EMT-like response.

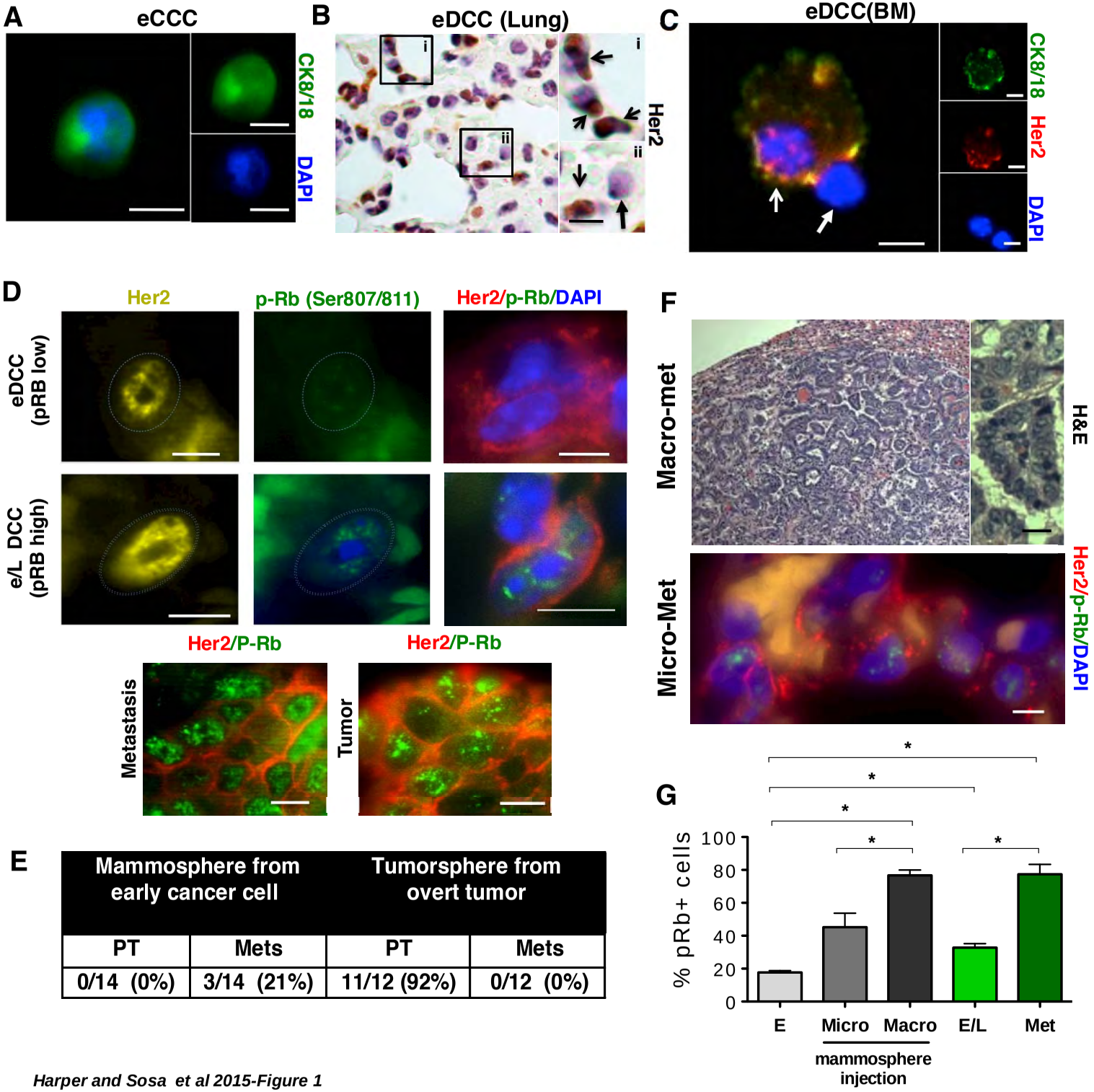

E

Mammosphere from early cancer cell		Tumorsphere from overt tumor	
PT	Mets	PT	Mets
0/14 (0%)	3/14 (21%)	11/12 (92%)	0/12 (0%)

Harper and Sosa et al 2015-Figure 1

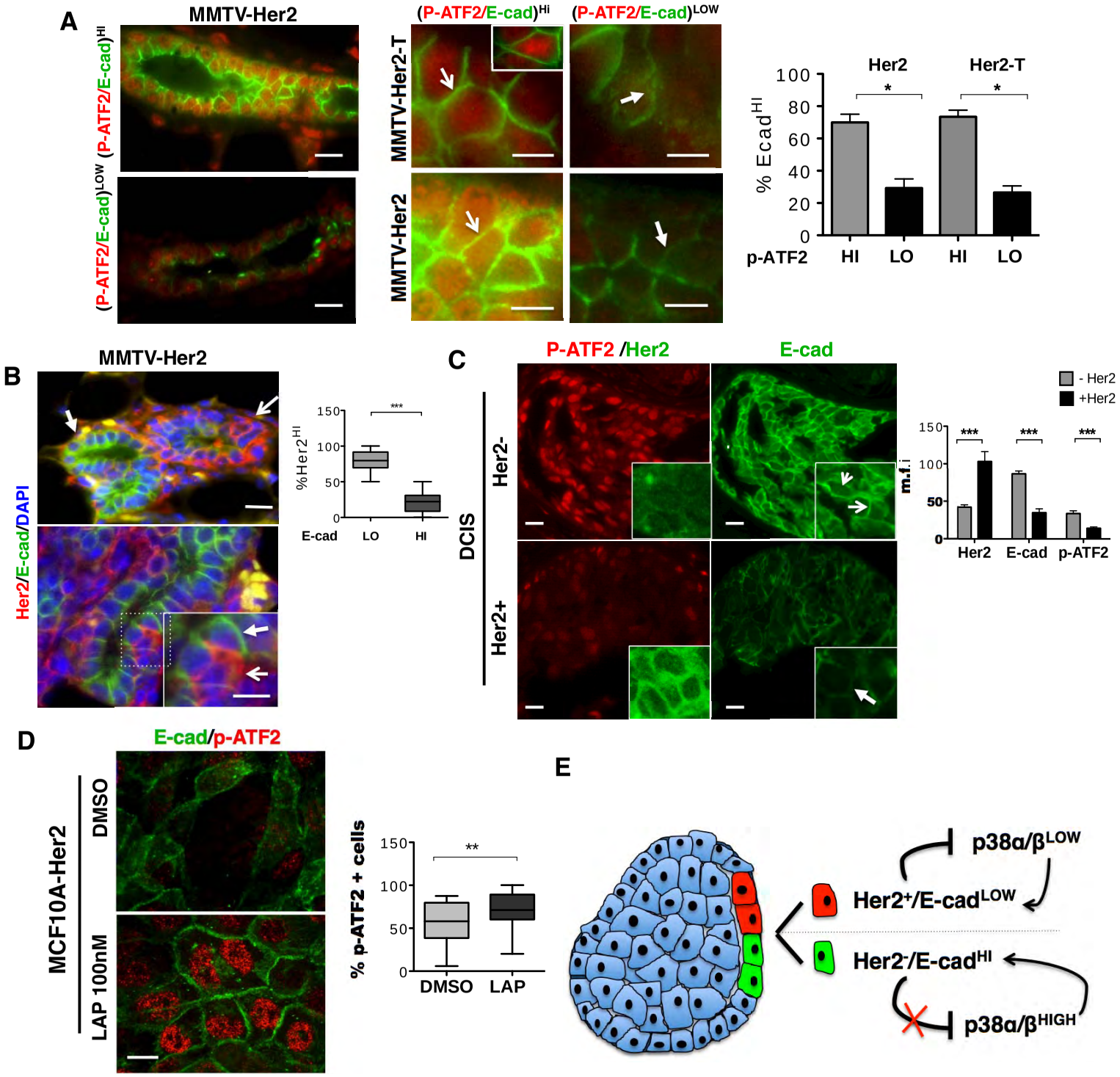

Harper and Sosa et al 2015-Figure 2

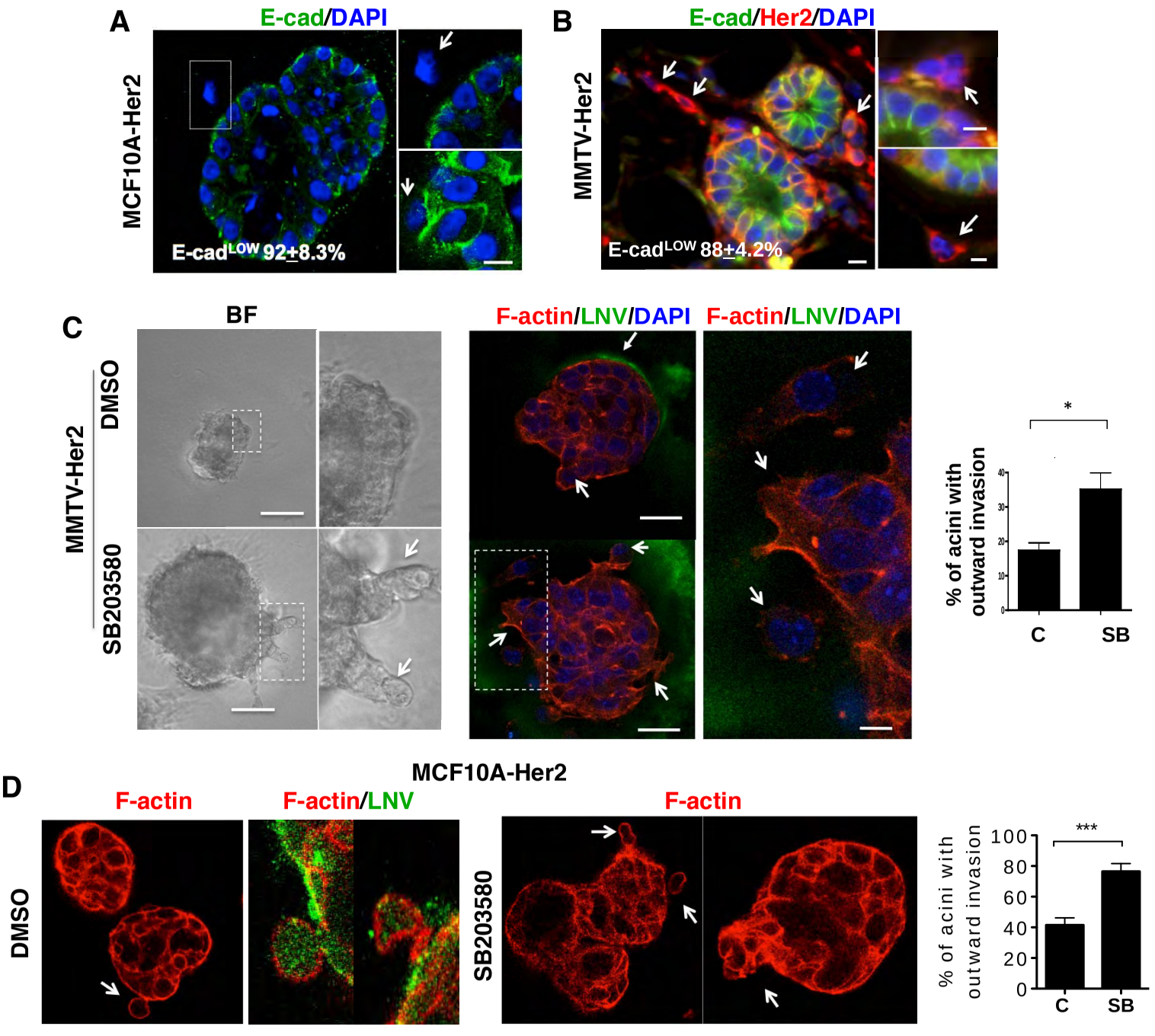

Harper and Sosa et al 2015-Figure 3

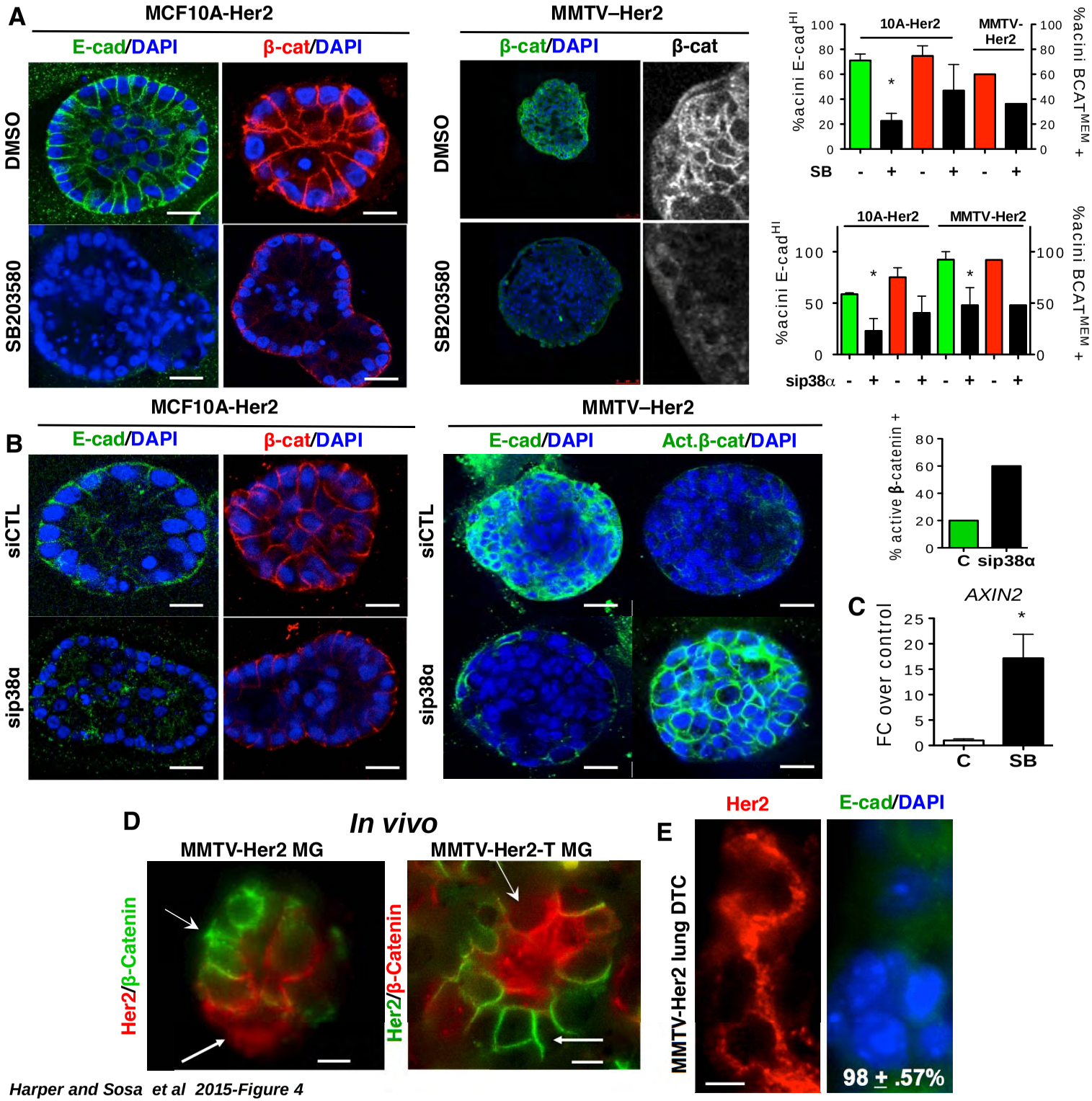

Harper and Sosa et al 2015-Figure 4

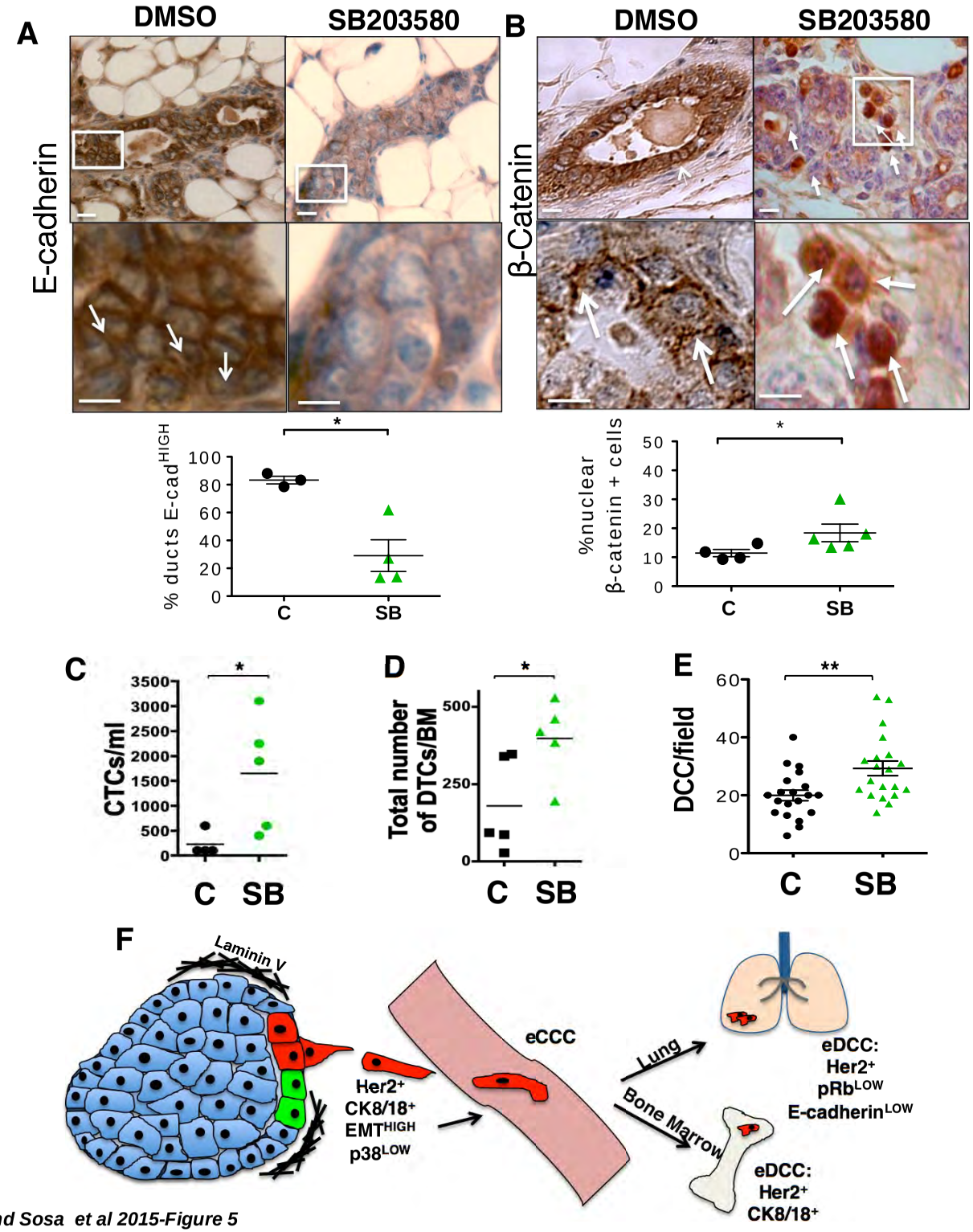

Harper and Sosa et al 2015-Figure 5

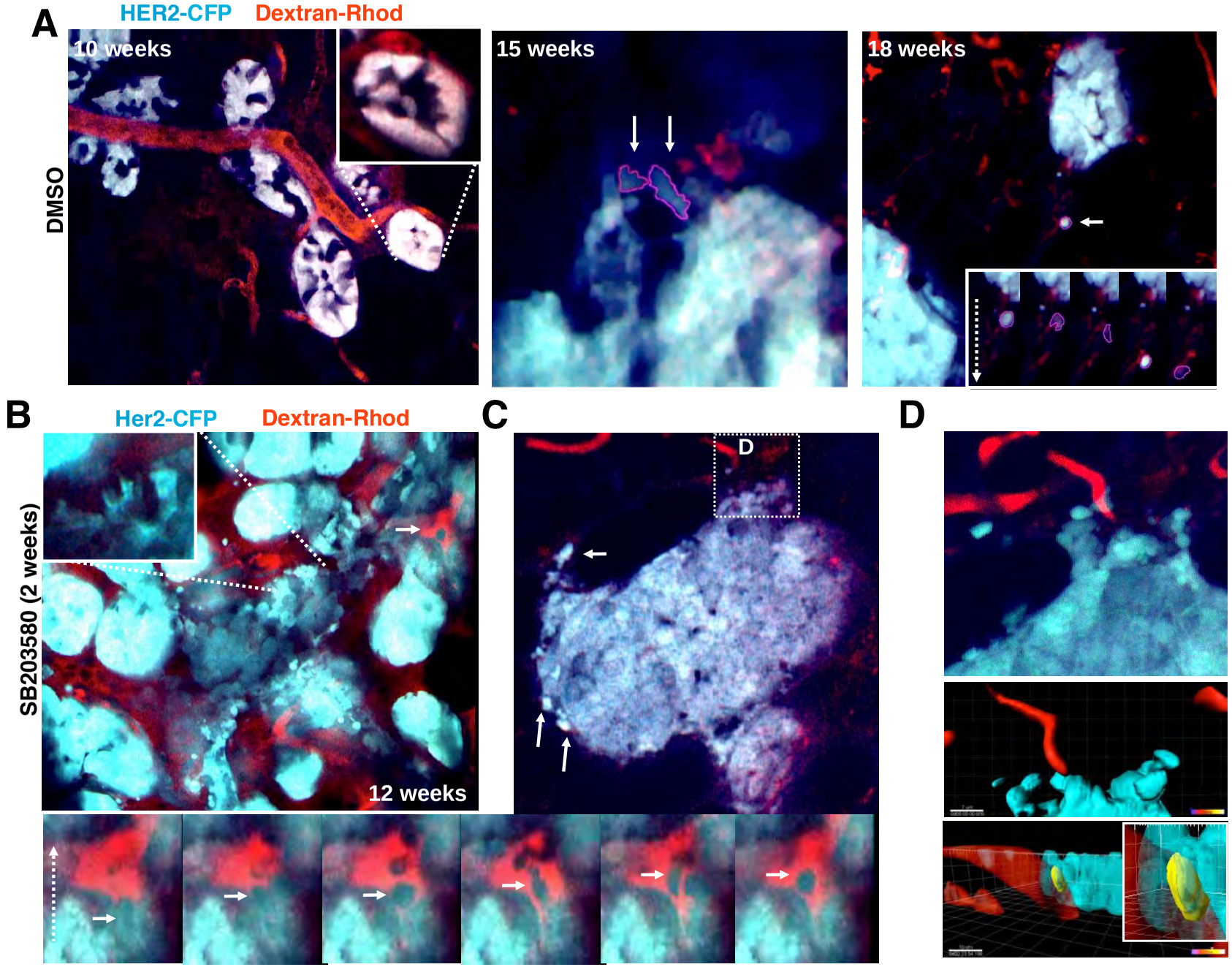

Harper and Sosa et al 2015-Figure 6

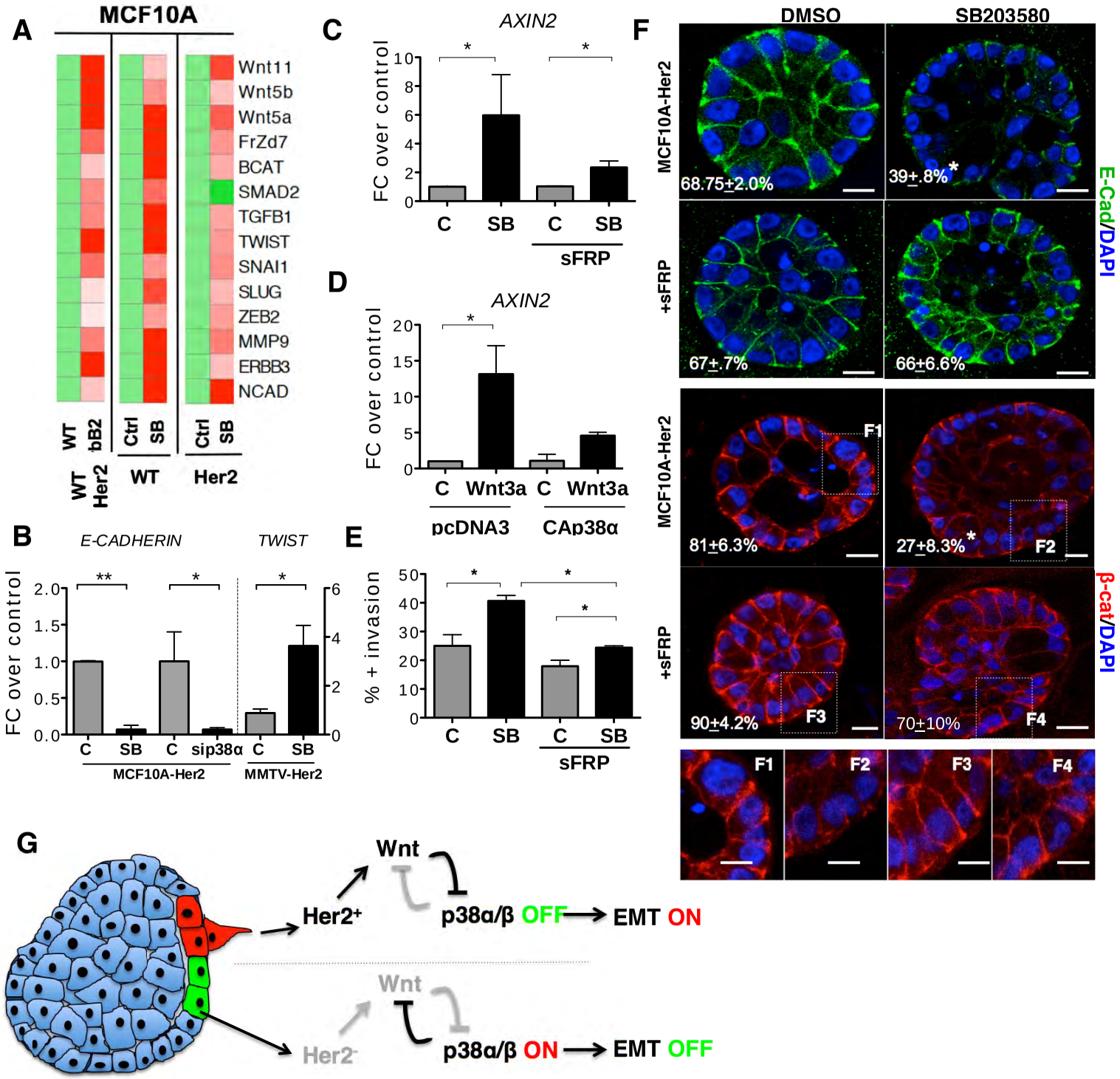

Harper and Sosa et al 2015-Figure 7